ELSEVIER

Colloids and Surfaces
A: Physicochemical and Engineering Aspects 192 (2001) 267–306

COLLOIDS AND SURFACES A

www.elsevier.com/locate/colsurfa

New developments in acoustic and electroacoustic spectroscopy for characterizing concentrated dispersions

Andrei S. Dukhin *, Philip J. Goetz

Dispersion Technology Inc., 3 Hillside Avenue, Mount Kisco, NY 10549, USA

Abstract

There are two different techniques (acoustics and electroacoustics), both of which employ ultrasound instead of light for characterizing properties of liquid-based dispersions. Acoustic and electroacoustic techniques offer a unique opportunity to characterize concentrated dispersion in their natural states because ultrasound can propagate through samples that are not transparent for light. Elimination of a dilution step is crucial for an adequate characterization of liquid dispersions, especially when the high concentration leads to structured systems. The last 2 years have been very successful for these new techniques. We give a short overview of the new developments during this time. It includes first of all a new electroacoustic theory which is valid for concentrated dispersions. So far this theory works only for thin double layer but for any value of the Dukhin number. Acoustic theory has been expanded as well due to incorporation of the 'structural losses' in addition to the existing mechanisms of the particles interaction with the sound field. There is a version now which is supposed to work in the structured dispersions. We give here the first example of this new application for acoustics. Another important new application for acoustics is a 'mixed dispersions', which is dispersed system with several dispersed phases. A specially developed 'effective media' approach allows us to tackle successfully these very complicated systems. Hardware has been improved during last 2 years as well. We mention here just one new device: ζ-potential probe. It makes electrokinetic measurement very simple, fast (down to 15 s), precise (0.1 mv) and accurate. It can work on-line. We give here some examples of the results obtained with this probe.

Keywords: Acoustic and electroacoustic spectroscopy; Dispersions; Colloidal

1. Introduction

Last 2 years was the time of the intensive growth of the new ultrasound based techniques for characterizing heterogeneous colloidal systems. New theories have been developed and new instruments became available. We are going to describe shortly these new developments in this paper.

The first technique described here is referred to as 'acoustics'. It is somewhat simpler than the second, which is referred to as 'electroacoustics'. Acoustics deals only with the acoustics properties of the dispersion such as the 'attenuation' and 'sound speed'. Electroacoustics is more complicated because it is related to the coupling between the acoustic and electric properties of the dispersion.

* Corresponding author. Tel.: +1-914-2414777; fax: +1-914-2414842.

0927-7757/01/$ - see front matter
PII: S0927-7757(01)00730-0

The history of the acoustics can be traced back to the creation of the first hardware for measuring the acoustic properties of liquids more than 50 years ago at MIT [1] by Pellam and Galt. The first attempt to develop an acoustic theory for heterogeneous systems was by Sewell 90 years ago [2], whereas the general acoustic principles for dilute systems were successfully formulated 45 years ago by Epstein and Carhart [3]. A long list of applications and experiments using acoustic spectroscopy appears in several reviews. [4,5]. Despite all these developments, acoustic spectroscopy is rarely mentioned in modern handbooks of colloid science [6,7].

Acoustics can provide reliable particle size information for concentrated dispersions without any dilution. There are examples for which acoustics yields size information at volume fractions above 40%. Such in situ characterization of concentrated systems makes the acoustic method very useful and quite unique compared to alternative methods including light scattering where extreme dilution is usually required. Acoustics is also able to deal with low dispersed phase volume fractions and some systems can be characterized at less than 0.1 vol.%. This flexibility in concentration range provides an important overlap with classical methods.

Acoustics does not require calibration with a known colloid. It is calibrated on first principles and provides an absolute particle size distribution (within the constraints of the model). It is a big advantage over modern back-light scattering technique which is also supposed to work in moderate concentrated dispersions [8]. In addition, acoustics theory of takes into account particle interaction [9] whereas back-light scattering technique is lacking such a theory.

Acoustics is more suitable than light scattering methods for characterizing polydisperse systems. Acoustics yields particle size on a weight basis which makes it similar to sedimentation techniques. Light scattering methods are much more sensitive to the presence of larger particles because this phenomenon exhibits a stronger dependence on the particle size, such as fifth or sixth power. As a result light scattering methods tend to overestimate the amount of larger particles and are often not able to resolve the presence of small particles in very polydisperse systems.

In addition to particle size, acoustics can also provide information about the microstructure of dispersed systems. The acoustic spectrometer can be considered as a micro-rheometer. Unlike traditional rheometers, an acoustic spectrometer applies stresses over a very short distance, on the scale of microns, thus sensing the microstructure of the dispersed system. This feature of acoustics is only beginning to be exploited.

The operating principles of the acoustic spectrometer are quite simple. The acoustic spectrometer generates sound pulses that after passing through a sample are measured by a receiver. The passage through the sample system causes the sound energy to change in intensity and phase. The acoustic instrument measures the sound energy losses (attenuation) and the sound speed. The sound attenuates due to the interaction with the particles and liquid in the sample system. Acoustic spectrometers work generally in the frequency range of 1–100 MHz. This is a much higher sound frequency than the upper limit of our hearing which is approximately 0.02 MHz. Acoustic spectrometer is non-destructive, energy of the ultrasound is very low in contrast with traditional sonicators built for eliminating aggregation.

While the operating principles are relatively simple, the analysis of the attenuation data to obtain particle size distributions does involve a degree of complexity, since the experimental results must be fitted to rather complex theoretical models based on various acoustic loss mechanisms. The advent of high speed computers and the refinement of these theoretical models have made the inherent complexity of this analysis of little consequence. In comparison, many other particle sizing techniques such as photon correlation spectroscopy also rely on similar levels of complexity in analyzing the experimental results.

Acoustic methods are very robust and precise [10]. They are much less sensitive to contamination compared to the traditional light-based techniques because the high concentration of particles in the fresh sample dominates any small residue from the previous sample. It is a relatively fast

techniques as well. Normally one particle size measurement can be done in a few minutes. This features make acoustic very attractive for on-line particle size monitoring.

Electroacoustics is a relatively new technique comparing to acoustics. The first reference to an electroacoustic effect was made by Debye [11] and there are several short historical reviews [12,13]. Electroacoustics is more complex than acoustics because an additional electric field is involved. Electroacoustics, in principle, can provide particle size information as well as zeta potential. There are two different implementations of electroacoustics, depending on which field is used as the driving force. Electrokinetic Sonic Amplitude (ESA) involves the generation of sound energy caused by the driving force of an applied electric field. Colloid Vibration Current (CVI) is the phenomenon where sound energy is applied to a system and a resultant electric field or current is created by the vibration of the colloid electric double layers.

There are two different opinions about the application of ultrasound based techniques to characterizing colloidal dispersions discussed in the paper [14]. We believe that acoustics is much more powerful than electroacoustics for particle size characterization. At the same time electroacoustics is the wonderful tool for ζ-potential characterization. We gave several positive arguments supporting our viewpoint years ago in the paper [14]. Here we repeat them with some additions resulting from our long time experience (Table 1).

Table 1
Advantages of the acoustics over the electroacoustics for particle sizing

1	No calibration using colloid with the known particle size
2	Much wider particle size range from 10 nm to 100 μ, comparing to the typical electroacoustic range from 100 nm to 10 μ
3	Particle size is independent on the any assumptions and any influence of the particles Double Layers
4	Particle sizing of uncharged particles
5	Particle size at high conductivity
6	Much less sensitive to the temperature variation
7	Much less sensitive to contamination

Table 2
Advantages of the electroacoustics over microelectrophoresis for ζ-potential characterization

1	No dilution, volume fraction up to 50%
2	Less sensitive to contamination
3	Higher precision (± 0.1 mV)
4	Low surface charges (down to 0.1 mV)
5	Electrosmotic flow is not important
6	Convection is not important
7	Accurate for non-aqueous dispersions

Taking into account these arguments we suggested the combination of acoustics and electroacoustics. According to this scheme, acoustics provides the particle size distribution whereas electroacoustics is used only for ζ-potential characterization. We would like to stress here that electroacoustics has many advantages over traditional microelectrophoretic method of the ζ-potential measurement. These advantages are summarized in the Table 2.

Interaction of ultrasound with a heterogeneous dispersed system involves various thermodynamic, hydrodynamic and electrodynamic effects. General theoretical picture is rather complex, however, there is always an opportunity to apply some simplification in the case of the particular real dispersion. This fortunate feature of acoustics historically has been implemented in terms of various mechanisms of the ultrasound interactions with a dispersed system. All together six mechanisms are known: (1) viscous; (2) thermal; (3) scattering; (4) intrinsic; (5) structural; and (6) electrokinetic.

(1) The 'viscous' mechanism is hydrodynamic in nature. It is related to the shear waves generated by the particle oscillating in the acoustic pressure field. These shear waves appear because of the difference in the densities of the particles and medium. The density contrast causes the particle motion with respect to the medium. As a result, the liquid layers in the particle vicinity slide relative to each other. The sliding non-stationary motion of the liquid near the particle is referred to as the 'shear wave'. This mechanism is important for acoustics. It causes losses of the acoustic energy due to the shear friction. Viscous dissipative losses are dominant for small rigid particles

with sizes below 3 μ, such as oxides, pigments, paints, ceramics, cement, and graphite.

Viscous mechanism is closely related to the electrokinetic mechanism which is also associated with the shear waves.

(2) The 'thermal' mechanism is thermodynamic in nature and it is related to the temperature gradients generated near the particle surface. Temperature gradients are due to the thermodynamic coupling between pressure and temperature. This mechanism is also important for acoustics. Dissipation of the acoustic energy caused by thermal losses is the dominant attenuation effect for soft particles, including emulsion droplets and latex beads.

For yet unknown reasons this thermodynamic effect does not show up in electroacoustics. There is a hypothesis [13] that it might be explained by different symmetry of thermodynamic and electrodynamic fields which eliminates their coupling.

(3) The 'scattering' mechanism is essentially the same as in the case of the light scattering. Acoustic scattering does not produce dissipation of acoustic energy. Particles simply redirect a part of the acoustic energy flow and as a result this portion of the sound does not reach the sound transducer. Scattering mechanism contributes to the overall attenuation and is important for acoustics. This contribution is significant for larger particles (>3 μ) and high frequency (>10 MHz).

(4) The 'intrinsic' mechanism is the part of acoustics. It causes losses of the acoustic energy due to the interaction of the sound wave with the materials of the particles and medium as homogeneous phases on a molecular level. It must be taken into account when overall attenuation is low which might happened for the small particles or low volume fractions.

(5) The 'structural' mechanism bridges acoustics with reology. Actually one can consider acoustic spectrometer as microreometer. In both cases we apply stress and measure respond. The difference is a scale of the applied stress. In the case of acoustics we apply stress over a half wavelength which is only about tenths of microns on the megahertz scale. Structural mechanism might contribute to the acoustic attenuation. Unfortunately, this mechanism is still well described.

(6) The 'electrokinetic' mechanism describes interaction of the ultrasound with the double layer of particles. Oscillation of charged particles in the acoustic field leads to the generation of an alternating electrical field, and consequently to alternating electric current. This mechanism is a basis for elerctroacoustics. It turned out its contribution to the acoustic attenuation is negligible. It is very important feature of acoustics because it makes it independent on the electric properties of the dispersion including properties of the double layers.

There is no theory which would take into account all six mechanisms. Derivation of such a theory is complicated by possible coupling between various mechanisms. Particle–particle interaction brings an additional factor which must be considered in the concentrated systems. Fortunately, there is an opportunity to simplify this theory dramatically applying so called 'long wave requirement' [15] which requires the wavelength of the sound wave λ to be larger than particle radius a.

$$\lambda >> a. \tag{1}$$

The 'long wave requirement' (Eq. (1)) restricts particle size for a given set of frequencies. Our experience shows that particle size must be below several tenths of microns for the frequency range from 1 to 100 MHz. This restriction is helpful for characterizing small particles.

Long wave requirement allows us to consider all mechanisms separately. For instance, we can express the total attenuation measured with the acoustic spectrometer α as a the sum of these five partial attenuations:

$$\alpha = \alpha_{vis} + \alpha_{th} + \alpha_{sc} + \alpha_{int} + \alpha_{str}, \tag{2}$$

where α_{vis} is the contribution of the viscous mechanism, α_{th} is the contribution of the thermal mechanism, α_{sc} is the contribution of the scattering mechanism, α_{int} is the attenuation in the pure liquid and α_{str} is the attenuation caused by oscillation of the particles bounds in the structured dispersion.

There is another approach to acoustics that employs a 'short wave requirement.' It was introduced by Riebel [16]. This approach works only

for large particles above 10 μ and requires limited input data about the sample.

Adopting long wave requirement allows us to use a 'coupled phase model' [9,17,18] for describing relative motion of the particles and liquid and 'cell model concept' [19,20,25,26] for incorporating hydrodynamic and electrodynamic particle interaction. These two useful theoretical methods are described below.

This review describes the present state of both acoustics and electroacoustics. We give here a short overview of the modern theory using the same basic notions and principles for both acoustics and electroacoustics. Then, we describe experimental tests that have been performed in order to verify this theory. At the end we give some examples that illustrate the usefulness of these ultrasound based techniques for characterizing real dispersions.

2. Coupled phase model

Let us consider the infinite small volume element in the dispersed system. There is a differential force acting on this element proportional to the pressure gradient of the sound wave ∇P. This external force is applied to both the particles and liquid and is distributed between particles and liquid according to the volume fraction φ.

Both particles and liquid move with an acceleration created by the sound wave pressure gradient. In addition, because of inertia effects, the particles move relative to the liquid which causes viscous friction forces acting between the particles and liquid.

The balance of these forces can be presented using the following system of equations written separately for particles and liquid:

$$-\varphi\ \nabla P = \varphi\ \rho_{\mathrm{p}} \frac{\partial u_{\mathrm{p}}}{\partial t} + \gamma(u_{\mathrm{p}} - u_{\mathrm{m}}), \tag{3}$$

$$-(1-\varphi)\nabla P = (1-\varphi)\ \rho_{\mathrm{m}} \frac{\partial u_{\mathrm{m}}}{\partial t} - \gamma(u_{\mathrm{p}} - u_{\mathrm{m}}), \tag{4}$$

where u_{m}, and u_{p} are velocities of the medium and particles in the laboratory frame of references, t is time and γ is a friction coefficient which is proportional to the volume fraction and particle hydrodynamic drag coefficient Ω,

$$\gamma = \frac{9\eta\varphi\ \Omega}{2a^2},$$

$$F_{\mathrm{f}} = 6\pi\ \eta\ a\Omega(u_{\mathrm{p}} - u_{\mathrm{m}}),$$

where η is dynamic viscosity, and a is the particles radius.

In addition we can use the mass conservation law which might be presented as follows:

$$-\frac{\partial P}{\partial t} = M^*(1-\varphi)\nabla u_{\mathrm{m}} + M^*\varphi\ \nabla u_{\mathrm{p}}, \tag{5}$$

where M^* is a stress modulus (the reciprocal of compressibility) of the dispersed system, t is a time.

The system of Eqs. (3)–(5) is well known in the field of acoustics. It has been used in several papers [9,17,18] for calculating sound speed and acoustic attenuation. It is valid without any restriction on volume fraction. Importantly, it is known that this system of equations yields a correct transition to the dilute case.

This system of equations is normally referred to as the 'coupled phase model'. The word 'model' usually suggests the existence of some alternative formulation, but it is hard to imagine what one can change in this set of force balance equations, which essentially express Newton's second law. Perhaps, the word 'model' is too pessimistic in this case.

The 'coupled phase model' opens an opportunity to describe polydisperse system without using superposition assumption. In order to do this we have to reformulate equations of the force balance for the polydisperse system.

Let us assume now that we have polydisperse system with conventional N fractions. Each fraction of particles has certain particle diameter d_i, volume fraction φ_i, drag coefficient γ_i, particle velocity u_i in laboratory frame of references. We assume density of the particles to be the same for all fractions ρ_{p}. Total volume fraction of the dispersed phase is φ. Liquid is characterized by dynamic viscosity η, density ρ_{m} and velocity in the laboratory frame of references u_{m}.

Coupled phase model suggests to apply force balance to each fraction of the dispersed system including dispersion medium. We did it before for one fraction. Now we apply the same principle to the N fractions. In addition we consider time and space dependence of the unknown field variables P, u_m and u_p as a monochromatic wave $A e^{j(\omega t - lx)}$, where j is a complex unit, l is a complex wavenumber, ω is a frequency of the ultrasound. As a result we obtain the following system of $N+1$ equations:

$$-\varphi_1 \nabla P = \varphi_1 \rho_p j\omega u_1 + \gamma_1 (u_1 - u_m)$$

$$\vdots$$

$$-\varphi_i \nabla P = \varphi_i \rho_p j\omega u_i + \gamma_i (u_i - u_m)$$

N equations for particles, (6)

$$-(1-\varphi)\nabla P = (1-\varphi)\rho_m j\omega u_m - \sum_i \gamma_i (u_i - u_m)$$

equation for the liquid, (7)

where

$$\gamma_i = \frac{18\eta\varphi_i \Omega}{d_i^2}$$

$$F^i_{stockes} = 3\pi\eta d\Omega (u_i - u_m).$$

Coupled phase model [13] allows us to calculate the particle velocity relative to the liquid $(u_i - u_m)$ for each fraction without using superposition assumption. We can solve system of $N+1$ equations following our previous paper [13]. In order to do this we reformulate all equations introducing desirable quantities $x_i = u_i - u_m$ and eliminate parameter u_m using the last equation which specifies the liquid velocity in a form:

$$u_m = -\frac{\nabla P}{j\omega\rho_m} + \frac{\sum_i \gamma_i x_i}{(1-\varphi)j\omega\rho_m}. \quad (8)$$

The new system of N equations is:

$$\left(\frac{\rho_p}{\rho_m} - 1\right)\nabla P = \left(j\omega\rho_p + \frac{\gamma_i}{\varphi_i}\right)x_i + \frac{\rho_p}{(1-\varphi)\rho_m}\sum_i \gamma_i x_i. \quad (9)$$

This system can be solved using the principle of mathematical induction. We guess solution for N fractions and then prove that the same solution works for $N+1$ fraction. As a result we obtain the following expression for velocity of the i-th fraction particle relative to the liquid:

$$u_i - u_m = \frac{(\rho_p/\rho_m - 1)\nabla P}{(j\omega\rho_p + \gamma_i/\varphi_i)\left(1 + (\rho_p/(1-\varphi)\rho_m)\sum_{i=1}^{N} \gamma_i/(j\omega\rho_p + \gamma_i/\varphi_i)\right)}. \quad (10)$$

This particle velocity is important for the further calculation in the electroacoustic theory. At the same time the 'coupled phase model' yields an important result for the acoustic theory. System of Eqs. (6) and (7) combined with the mass conservation law allows us to calculate the complex wavenumber without using superposition assumption. This was done in the paper [9]. We reproduce the result here:

$$\frac{l^2 M^*}{\omega^2} = \frac{(1-\varphi)\rho_m + \sum_{i=1}^{N} \gamma_i (\mathrm{Den}_i - j\omega\gamma_i)/j\omega\mathrm{Den}_i}{\left(1 - \varphi + \sum_{i=1}^{N} \frac{j\omega\varphi_i\gamma_i}{\mathrm{Den}_i}\right)^2 - \sum_{i=1}^{N} (\omega^2\varphi_i^2/\mathrm{Den}_i)\left(\rho_m - \varphi\rho_m + \sum_{i=1}^{N} \gamma_i(\mathrm{Den}_i - j\omega\gamma_i)/j\omega\mathrm{Den}_i\right)}, \quad (11)$$

where

$$\mathrm{Den}_i = -\omega^2\varphi_i\rho_p + j\omega\gamma_i + j\omega\delta_i + \beta_i.$$

Parameters β_i and δ_i are two first virial coefficients which characterize oscillation of the structure in the case when particles are bound. These parameters links this theory to the reology. We show in this review following paper [52] how to use these parameters on the example of the real structured concentrated dispersions of alumina.

Figs. 1 and 2 illustrate effect of the structure on the attenuation spectra of 40 vol.% alumina dispersion with median size 1 μ. It is seen that the

first virial coefficient just shifts the critical frequency, keeping the shape of the curve more or less intact and the peak attenuation constant. Since the particle size is reciprocally proportional to the square root of this critical frequency, the influence of the structure must be very substantial in order to create large errors in the particle size.

Influence of the first virial coefficient could not affect quality of fitting. For instance, it cannot explain possible excess attenuation. Elastic structure does not change the amplitude of attenuation.

In principle, this second virial coefficient can be extracted from the attenuation spectra as an adjustable parameter as it is shown below.

Expression 11 specifies the complex wavenumber neglecting thermodynamic effects. There is a versions of the coupled phase model which take into account thermodynamic effects as well [21]. It is important in the case of the flexible particles when the 'thermal' mechanism becomes significant.

Coupled phase model does not assume the absence of the particle–particle interaction. Parameters β_i and δ_i reflect the specific particles interaction like polymer bounds whereas the hydrodynamic particle–particle interaction is incorporated into the drag coefficient γ. We can take into account this hydrodynamic effect calculating γ using 'cell model concept' which is described in the following section.

3. Cell model concept

The main idea of the 'cell model' is that each particle in the concentrated system is considered separately inside of spherical cell of liquid associated only with given individual particle. The cell boundary conditions formulated on the outer boundary of the cell reflect the particle–particle interaction.

In the past, the cell model has been applied only to monodisperse systems. This restriction allows one to define the radius of the cell. Equating the solid volume fraction of the each cell to the volume fraction of the entire system yields the following expression for the cell radius b:

$$b = \frac{a}{\sqrt[3]{\varphi}}. \tag{12}$$

In the case of a polydisperse system, the intro-

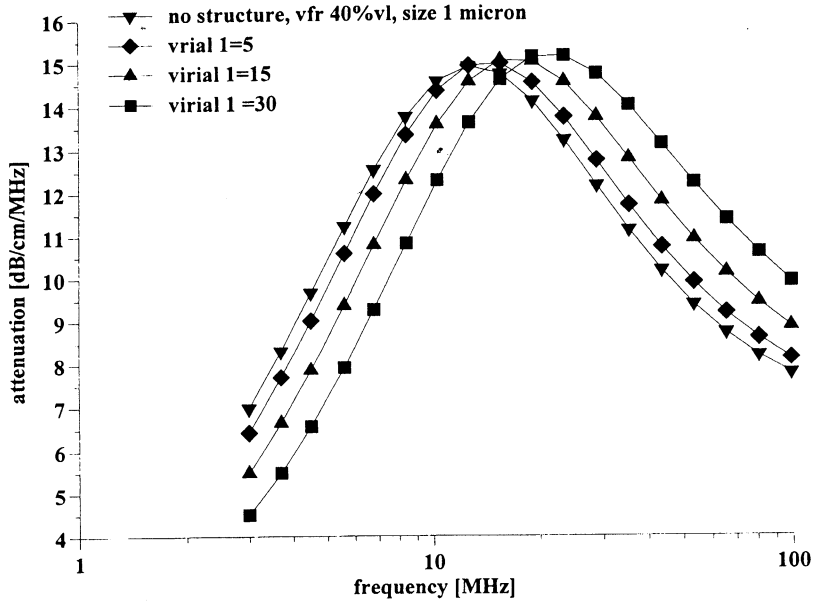

Fig. 1. Theoretical attenuation of the 40 vol.% alumina slurry with 1 μ particles at different values of the first virial coefficient assuming the second virial coefficient to be a zero.

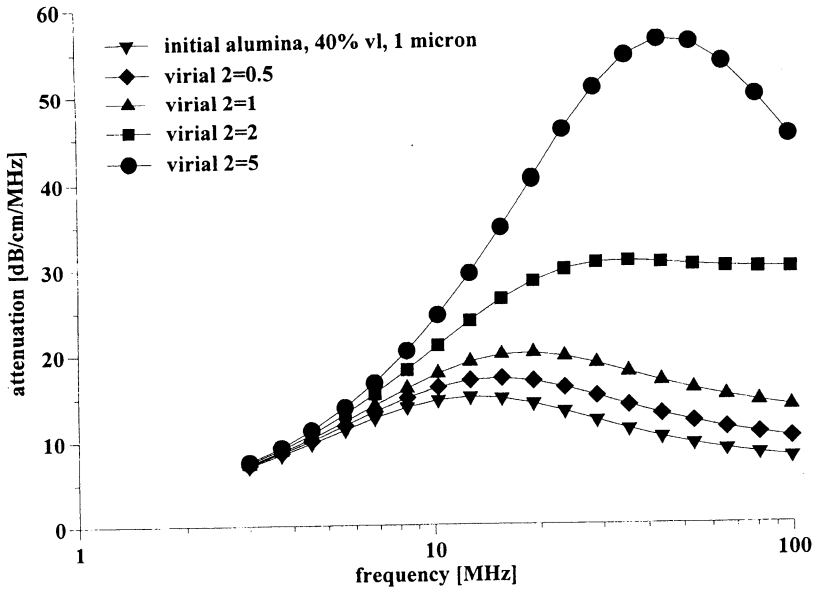

Fig. 2. Theoretical attenuation of the 40 vol.% alumina slurry with 1 μ particles at different values of the second virial coefficient assuming the first virial coefficient to be a zero.

duction of the cell is more complicated because the liquid can be distributed between fractions in an infinite number of ways. However, the condition of mass conservation is still necessary.

Each fraction can be characterized by particles radii a_i, cell radii b_i, thickness of the liquid shell in the spherical cell $l_i = b_i - a_i$ and volume fraction φ_i. The mass conservation law relates these parameters together as follows:

$$\sum_{i=1}^{N}\left(1+\frac{l_i}{a_i}\right)^3\varphi_i = 1. \tag{13}$$

This expression might be considered as an equation with N unknown parameters l_i. An additional assumption is still necessary to determine the cell properties for the polydisperse system. This additional assumption should define the relationship between particle radii and shell thickness for each fraction. We suggest the following simple relationship:

$$l_i = la_i^n. \tag{14}$$

This assumption reduces the number of unknown parameters to only two which are related by the following expression:

$$\sum_{i=1}^{N}(1+la_i^{n-1})^3\varphi_i = 1. \tag{15}$$

The parameter n is referred to as a 'shell factor'. Two specific values of the shell factor correspond to easily understood cases. A shell factor of 0 depicts the case in which the thickness of the liquid layer is independent on the particle size. A shell factor of 1 corresponds to the normal 'superposition assumption' which gives the same relationship between particles and cell radiuses in the monodisperse case, i.e. each particle is surrounded by a liquid shell which provides each particle the same volume concentration as the volume concentration of the overall system.

In general, the 'shell factor' might be considered an adjustable parameter because it adjusts the dissipation of energy within the cells. However, our experience using this cell model with acoustics for particle sizing [22] indicates that shell factor equal 1 is almost always suitable. We take this value of n for the further derivations.

Cell model concept can be applied for describing the hydrodynamic effects as well as electrokinetc effects. The following sections present the short review of both types of the cell models.

4. Hydrodynamic cell model

There are two most widely used hydrodynamic cell model called according to the names of their authors: Happel cell model [23] and Kuwabara cell model [24]. Both of these are formulated for incompressible liquid. The long wavelength requirement (Eq. (1)) allows us to use this traditional hydrodynamics in the non-stationary case of the ultrasound field. The system of the equations for liquid velocity u and hydrodynamic pressure P is as following:

$$\rho_m \frac{du}{dt} = \eta \text{ rot rot } u + \text{grad } P, \tag{16}$$

$$\text{div } u = 0. \tag{17}$$

Both models apply the same boundary conditions at the surface of the particle:

$$u_r(r=a) = u_p - u_m, \tag{18}$$

$$u_\theta(r=a) = -(u_p - u_m). \tag{19}$$

The boundary conditions at the surface of the cell are different. For the Kuvabara cell model it is given by the following equations:

$$\text{rot } u_{r=b} = 0, \tag{20}$$

$$u_r(r=b) = 0. \tag{21}$$

In the case of the Happel cell model they are:

$$\prod_{r\theta}(r=b) = \frac{1}{r}\frac{\partial u_r}{\partial \theta} + r\frac{\partial (u_\theta/r)}{\partial r} = 0, \tag{22}$$

$$u_r(r=b) = 0. \tag{23}$$

The general solution for the velocity field contains three unknown constants C, C_1 and C_2:

$$u_r(r) = C\left(1 - \frac{b^3}{r^3}\right) + 1.5\int_r^b \left(1 - \frac{x^3}{r^3}\right) h(x)\,dx, \tag{24}$$

$$u_\theta(r) = -C\left(1 + \frac{b^3}{2r^3}\right) - 1.5\int_r^b \left(1 + \frac{x^3}{2r^3}\right) h(x)\,dx, \tag{25}$$

$$h(x) = C_1 h_1(x) + C_2 h_2(x). \tag{26}$$

The drag coefficient can be expressed in the following form general for both Kuvabara and Happel cell models:

$$\Omega = -\frac{\alpha^2}{3}\left(\frac{d(C_1 h_1 + C_2 h_2)}{dx} + \frac{C_1 h_1 + C_2 h_2}{\alpha}\right)_{x=\alpha} - \frac{4j\alpha^2}{9}, \tag{27}$$

where x is normalized same way as α, coefficients C_1 and C_2 are different for two cell models:

	Kuvabara	Happel
C_1	$\frac{h_2(b)}{I}$	$\frac{bh_2(b)-2I_{23}}{bI+2(I_2I_{13}-I_1I_{23})}$
C_2	$-\frac{h_1(b)}{I}$	$-\frac{bh_1(b)-2I_{13}}{bI+2(I_2I_{13}-I_1I_{23})}$

Happel cell model suits more for acoustics because it describes more adequately energy dissipation, whereas Kuvabara cell model is better for electroacoustics because it automatically yields Onsager relationship [20,25].

5. Electrokinetic cell model

Electrokinetic cell models are the results of some generalization of the hydrodynamic cell models. There are many ways to perform this generalization and, correspondingly, many ways to create a different electrokinetic cell models. The difference between electrokinetic cell models is related to the description of the electric characteristics. The relationship between macroscopic experimentally measured electric properties and local electric properties calculated using cell concept varies for different cell models. For instance, Levine–Neale cell model [27] specifies this relationship using one of the many possible analogies between local and macroscopic properties. Macroscopic properties are current density $\langle I\rangle$ and electric field strength $\langle E\rangle$. They are related with local electric current density I and electric field $\nabla\phi$ according to the Levine–Neale cell model with following expressions:

$$\langle I\rangle = \frac{\phi}{b\cos\theta_{r=b}}, \tag{28}$$

$$\langle E\rangle = \frac{1}{\cos\theta}\frac{\partial\phi}{\partial r}_{r=b}. \quad (29)$$

Relationships Eqs. (28) and (29) are not unique. There are many other ways to relate macroscopic and local fields. It means that we need a set of criteria to select a proper cell model. These criteria have been suggested in the electrokinetic cell model created by Shilov and Zharkikh [25,26]. Their two criteria determine a proper choice of the macroscopic 'fields' and 'flows'.

The first criteria is a well-known Onsager relationship [6] which constrain values of the macroscopic particles velocity relative to the liquid $\langle V\rangle$, macroscopic pressure $\langle P\rangle$, electric current $\langle I\rangle$ and field $\langle E\rangle$:

$$\frac{\langle V\rangle}{\langle I\rangle_{\langle\nabla P\rangle=0}} = \frac{\langle E\rangle}{\langle\nabla P\rangle}^{\langle I\rangle=0}. \quad (30)$$

This relationship requires a certain expression for entropy production Σ:

$$\Sigma = \frac{1}{T}(\langle I\rangle\langle E\rangle + \langle V\rangle\langle\nabla P\rangle). \quad (31)$$

Shilov and Zharkikh used this relationship between 'fields','flows' and entropy production in order to derive cell model condition for macroscopic properties. It turned out that expression for the macroscopic field strength is different comparing with Levine–Neale:

$$\langle E\rangle = \frac{\phi}{b\cos\theta}^{r=b}, \quad (32)$$

whereas expression for the macroscopic current is the same in the both models.

This cell model yields the correct transition to the Smoluchowski law. Smoluchowski law is a very important test for any electrokinetic theory because it is valid for any geometry and volume fraction. Failure to satisfy the Smoluchowski law test is a clear indication that the theory is not correct. Shilov and Zharkikh wrote in their paper that their theory met Smoluchowski law requirement. They even made a stronger conclusion that it was the Levine–Neale cell model which did not reduce to the Smoluchowski law. This opinions is discussed in the paper [20]. It was shown again that this difference comes from the misunderstanding of the Smoluchowski law in the case of concentrated systems. The version of Smoluchowski law which is valid in concentrated systems confirms Shilov–Zharkikh cell model.

6. Theory of acoustics

The most well known acoustic theory for heterogeneous systems was developed by Epstein, Carhart [3], Allegra and Hawley [28]. The theory takes into account the four most important mechanisms (viscous, thermal, scattering and intrinsic) and is termed the 'ECAH theory.' It describes the acoustic attenuation for a monodisperse system of spherical particles and is valid only for dilute systems. Extensions of the ECAH theory to include polydispersity have typically assumed a simple linear superposition of the attenuation for each size fraction. The term 'spherical' is used to denote that all calculations are performed assuming that each particle can be adequately represented as a sphere.

Most importantly, the term 'dilute' is used to indicate the assumption that there are no particle–particle interactions. This fundamental limitation normally restricts the application of the resultant theory to dispersions with a volume fraction of less than a few volume percent. However, there is some evidence that the ECAH theory, in some very specific situations, does nevertheless provide a correct interpretation of experimental data, even for volume fractions surprisingly as large as 30%.

An early demonstration of this ability of the ECAH theory was provided by Allegra and Hawley. They observed almost perfect correlation between experiment and ECAH theory for following dispersions: a 20% by volume toluene emulsion; a 10% by volume hexadecane emulsion; and a 10% by volume polystyrene latex. Experiments with emulsions by McClements [29,30] has provided similar results. The recent work by Holmes, Challis and Wedlock [31,32] also shows good agreement between ECAH theory and experiments even for 30% by volume polystyrene latex. An absence of particle–particle interaction was also observed with neoprene latex [33].

It is important to note that the unexpected validity of the dilute ECAH theory for moderately concentrated systems has only been demonstrated in systems where the 'thermal losses' were dominant, such as emulsions and latex systems.

The difference between the 'viscous depth' and the 'thermal depth' provides an answer to the observed differences between emulsions and solid particle dispersions. These parameters characterize the penetration of the shear wave and thermal wave correspondingly into the liquid. Particles oscillating in the sound wave generate these waves which damp in the particle vicinity. The characteristic distance for the shear wave amplitude to decay is the 'viscous depth' δ_v. The corresponding distance for the thermal wave is the 'thermal depth' δ_t. The following expressions give values for the parameters in dilute systems:

$$\delta_n = \sqrt{\frac{2\nu}{\omega}}, \tag{33}$$

$$\delta_t = \sqrt{\frac{2\tau_m}{\omega\rho_m C_p^m}}, \tag{34}$$

where ν is the kinematic viscosity, ω is the sound frequency, ρ_m is the density, τ_m is heat conductance, C_p^m is a heat capacity at constant pressure of liquid.

The relationship between δ_v and δ_t has been considered before. For instance, McClements plots 'thermal depth' and 'viscous depth' versus frequency [29,30]. It is easy to show that the 'viscous depth' is 2.6 times more than the 'thermal depth' in aqueous dispersions. As a result, the particle viscous layers overlap at the lower volume fraction more than the particle thermal layers. Overlap of the boundary layers is the measure of the corresponding particle–particle interaction. There is no particle interaction when corresponding boundary layers are sufficiently separated.

Thus, an increase in the dispersed volume fraction for a given frequency first leads to the overlap of the viscous layers because they extend further into the liquid. Thermal layers overlap at higher volume fractions. Therefore, the particle hydrodynamic interaction becomes more important at the lower volume fractions than the particle thermodynamic interaction.

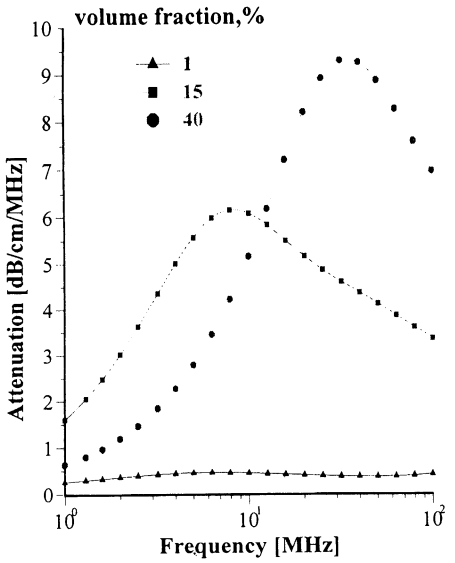

Fig. 3. Attenuation spectra calculated for various volume fractions of the dispersion of 1 μ particles.

Overlap of the boundary layers affects a critical frequency at which attenuation expressed in dB cm^{-1} per MHz reaches maximum. For systems where the viscous acoustic losses dominate, the maximum is shifted to higher frequencies at high concentrations, which will result in a lower attenuation value for a given frequency. Therefore if the attenuation is considered at a single frequency the attenuation will at first increase with higher dispersed phase. Once the concentration is high enough, the attenuation curve and maximum shift to higher frequencies and the attenuation at the considered single frequency decreases. This effect is illustrated with calculated attenuation spectra on Fig. 3 and later it is proved with equilibrium dilution test [13].

The 2.6 times difference between δ_v and δ_t leads to a large difference in the volume fractions corresponding to the beginning of the boundary layers overlap. It is interesting that this important feature of the 'thermal losses' works for almost all liquids [34,21]. Therefore 'thermal losses' are much less sensitive to the particle–particle interaction than 'viscous losses' for almost all known liquids. It makes ECAH theory valid in a much wider range of emulsion volume fractions than one would expect.

There is one fact that follows from the values of the liquid's thermal properties that makes it convenient to use ECAH theory. In general, ECAH theory requires information about three thermodynamic properties: thermal conductivity τ, heat capacity C_p and thermal expansion β. It turns out that τ and C_p are almost the same for all liquids except water [35]. The number of required parameters is then reduced to one — thermal expansion. The parameter of the thermal expansion then plays the same role in 'thermal losses' as density in 'viscous losses'.

ECAH theory has a big disadvantage of being mathematically complex. It cannot be generalized for particle–particle interactions. Long wave requirement allows us to overcome this problem by simplifying the theory. We can express the total attenuation measured with the acoustic spectrometer as a the sum of these five partial attenuations (see Eq. (2)) if long wave requirement is valid. In addition, by restricting frequency and particle size with the longwave requirement we can use the simpler explicit expression for the thermal losses α_{th} obtained initially by Isakovich [36] and confirmed later by Epstein and Carhart [3], Allegra and Hawley [28]:

$$\alpha_{th} = \frac{3\varphi T c_m \rho_m \tau_m}{2a^2}\left(\frac{\beta_m}{\rho_m C_p^m} - \frac{\beta_p}{\rho_p C_p^p}\right)^2 \mathrm{Re}\left(\frac{1}{1-jz_m} - \frac{\tau_m \tanh z_p}{\tau_p \tanh z_p - z_p}\right), \quad (35)$$

where

$$z = (1+j)\sqrt[a]{\frac{\omega\rho C_p}{2\tau}}.$$

At the same time the long wave requirement provides a sufficient simplification of the theory for taking into account particle–particle hydrodynamic interaction into the theory of the viscous losses. It has been done in the work [9] on the basis of the 'coupled phase model' [17,18]. This new theory works up to 40% volume and yields the following expression for the complex wavenumber l assuming viscous losses as the only one mechanism of the particles interaction with the sound wave:

$$\frac{l^2 M^*}{\omega^2} = \frac{\rho_m(1-\varphi) + \rho_p \sum_{i=1}^{N} \frac{\varphi_i \gamma_i}{(j\omega\rho_p\varphi_i + \gamma_i)}}{(1-\varphi)^2 + \sum_{i=1}^{N} \frac{(\varphi_i(\varphi-2)\gamma_i - \varphi_i^2(1-\varphi)\rho_m)}{j\omega\rho_p\varphi_i - \gamma_i}}, \quad (36)$$

where Ω is a drag coefficient specified above, M^* is stress modulus which can be expressed in terms of densities and sound speeds as follows:

$$M^* = \frac{\rho_p \rho_m c_p^2 c_m^2}{\varphi\rho_m c_m^2 + (1-\varphi)\rho_p c_p^2}$$

Expression Eq. (36) specifies the value of viscous losses:

$$c_{vis} = -\mathrm{Im} l \quad (37)$$

This theory can be used also for calculating sound speed of the dispersions where viscous losses are dominant.

$$c_s = \frac{\omega}{\mathrm{Re}\, l}. \quad (38)$$

Equation Eq. (36) neglects contribution from the specific forces or particle bonds. It means that it is valid only in non-structured dispersions. In the case of the structured dispersions the more general Eq. (11) must be used. That equation presents together contribution of the viscous and structural losses. It is interesting to consider an extreme case when viscous losses are negligible, but structural ones are dominant. It is case of the gels made either by very small nano-particles or by polymers. Eq. (11) yields the following expression for the structural losses of gels:

$$\frac{l^2 K^*}{\omega^2} = \frac{\rho_0(\beta - \omega^2\rho_p\varphi) + j\omega\delta\rho_0}{[(1-\varphi)(\beta - \omega^2\rho_p\varphi) - \omega^2\varphi^2\rho_0] + j(1-\varphi)\omega\delta}. \quad (39)$$

Expressions for calculating intrinsic α_{int} and scattering losses α_{sc} for long-wave limit are given in the papers of McClements [4,29,30]. He uses the term 'lossless scatterers' for describing sound propagation through the system when dissipative mechanisms of viscous and thermal losses are negligible. Intrinsic attenuation in such a system can be expressed as following [33]:

$$\alpha_{\text{int}} = \frac{(1-\varphi)(\alpha_{\text{m}}/c_{\text{m}}) + \varphi(\rho_{\text{m}}\alpha_{\text{p}}/\rho_{\text{p}}\alpha_{\text{m}})}{\sqrt{((1-\varphi)/c_{\text{m}}^2) + (\varphi\rho_{\text{m}}/\rho_{\text{p}}c_{\text{p}}^2)}} \sqrt{\frac{\rho_s}{\rho_{\text{m}}}}, \quad (40)$$

where α_{m} and α_{p} are attenuations of the medium and particle materials.

Scattering attenuation can be calculated following the Waterman–Truell theory [37] which yields the following expression for the complex wavenumber l_{s} associated with scattering:

$$\frac{l_{\text{s}}^2}{l_{\text{m}}^2} = \left(1 - \frac{3j\varphi}{(l_{\text{m}}a)^3} A_0\right)\left(1 - \frac{9j\varphi}{(l_{\text{m}}a)^3} A_1\right),$$

where A_0 and A_1 are monopole and dipole scattering coefficients calculated for a single particle,

$$l_s = \frac{\omega}{c_s} + j\alpha_{\text{sc}},$$

$$l_{\text{m}} = \frac{\omega}{c_{\text{m}}} + j\alpha_{\text{m}}.$$

The simplest formula expressing the scattering losses in terms of densities and sound speeds can be derived from Eq. (10) for a single scattering:

$$\alpha_{\text{sc}} = \frac{\varphi\omega^4 a^3}{2c_{\text{m}}^4}\left[\frac{1}{3}\left(1 - \frac{\rho_{\text{m}}c_{\text{m}}^2}{\rho_{\text{p}}c_{\text{p}}^2}\right)^2 + \left(\frac{\rho_{\text{p}} - \rho_{\text{m}}}{2\rho_{\text{p}} + \rho_{\text{m}}}\right)^2\right]. \quad (41)$$

It is seen that scattering losses depend on frequency very strongly. According to our experience scattering is important only for large particle (> 3 μ) and at high frequencies (> 10 MHz).

There are two recent developments in the theory of acoustics that deserve to be mentioned here. The first one is a theory of acoustics for flocculated emulsions [38]. It is based on ECAH theory but it uses in addition an 'effective medium' approach for calculating thermal properties of the flocs. The success of this idea is related to the feature of the thermal losses that allows for insignificant particle–particle interactions even at high volume fractions. This mechanism of acoustic energy dissipation does not require relative motion of the particle and liquid. Spherical symmetrical oscillation is the major term in these kind of losses. This provides the opportunity to replace the floc with an imaginary particle assuming a proper choice for the thermal expansion.

Another significant recent development is due to Samuel Temkin. He offers in his recent papers [39,40] a new approach to the acoustic theory. Instead of assuming a model dispersion consisting of spherical particles in a Newtonian liquid, he suggests that the thermodynamic approach is explored as far as possible. This new theory is based on particle velocities and temperature fluctuations. Tempkin's theory yields some unusual results, but has not yet been used in commercially available instruments.

7. Theory of electroacoustics

Whereas acoustic spectroscopy describes the combined effect of all loss mechanisms, electroacoustic spectroscopy, as it is presently formulated, emphasizes only electrokinetic mechanism.

In acoustic spectroscopy sound is utilized as both the excitation and the measured variable, and therefore there is but one basic implementation. In contrast, electroacoustic spectroscopy deals with the interaction of electric and acoustic fields and therefore there are two possible implementations. One can apply a sound field and measure the resultant electric current which is referred to as the colloid vibration current (CVI), or conversely one can apply an electric field and measure the resultant acoustic field which is referred to as the electronic sonic amplitude (ESA).

CVP occurs when the density of the particles ρ_{p} differs from that of the medium ρ_{m}, and the particles move relative to the medium under the influence of an acoustic wave. This motion causes a displacement of the internal and external parts of the double layer (DL) and is usually referred to as a polarization of the DL [44]. The displacement of opposite charges gives rise to a dipole moment and the superposition of the electric fields of these induced dipole moments over the collection of particles gives rise to a macroscopic electric current defined as the colloid vibration current (CVI). Thus, the fourth mechanism of particles interaction with sound leads to the transformation of part of the acoustic energy to electric energy. This electric energy may then be dissipated if the opportunity for electric current flow exists.

ESA occurs when an alternating electric field is applied to the disperse system [12]. If the zeta

potential of the particle is greater than zero, then the oscillating electrophoretic motion of the charged dispersed particles generates a sound wave. Both electroacoustic parameters CVI and ESA can be experimentally measured. The CVI or ESA spectrum is the experimental output from electroacoustic spectroscopy. Both of these spectra contain information about ζ-potential and PSD, however, only one of the electroacoustic spectra is required because both of them contain essentially the same information about the dispersed system.

The conversion of electroacoustic spectra into PSD requires a theoretical model of the electroacoustic phenomena. This conversion procedure is much more complicated for electroacoustics compared to acoustics because of the additional complications arising from the added electric field.

There are two quite different approaches to derive an electroacoustic theory. Historically the first began with works by Enderby and Booth [41,42]. They simply tried to solve a system of classical electrokinetic equations without using any thermodynamic relationships. It was very complex because they took into account surface conductivity effects. Although this initial theory was valid only for dilute systems, this approach was later expanded by Malrow, Fairhurst and Pendse [43], who tried to generalize it for concentrated systems using a Levine cell model. Unfortunately, this first attempt to create electroacoustic theory for concentrates was not successful because Levine cell model is not suitable for this purpose [13].

An alternative approach to electroacoustic theory was suggested later by O'Brien [45,46]. He introduced the concept of a dynamic electrophoretic mobility μ_d and suggested a relationship between this parameter and the measured electroacoustic parameters such as Colloid Vibration Current (CVI) or Electrosonic Amplitude (ESA):

$$\text{ESA (CVI)} = C_{\text{cal}} \frac{\rho_p - \rho_m}{\rho_m} \varphi \mu_d E(\nabla P), \qquad (42)$$

where C_{cal} is a cell constant, P is the hydrodynamic pressure, and E is the external electric field strength.

Unfortunately, the simple relationship Eq. (42) is not valid for concentrated systems as it was shown theoretically and experimentally in the work [13].

According to O'Brien's a complete functional dependence of ESA(CVI) on the key parameters like ζ-potential, particle size and frequency is incorporated into dynamic electrophoretic mobility. Coefficient of proportionality between ESA (CVI) and μ_d is frequency independent as well as is independent on particle size and ζ-potential. This peculiarity of the Eq. (42) made dynamic electrophoretic mobility being a central parameter of the electroacoustic theory.

The first theory of the dynamic electrophoretic mobility which relates this parameter with other properties of the dispersed system was created initially by O'Brien for dilute case only, neglecting particle–particle interaction. We call this version the 'dilute O'Brien's theory'.

Later he applied Levine cell model trying to expand dynamic electrophoretic theory to concentrated systems [46]. This work was generalized recently by Ohshima [47]. We call this version the 'O'Brien-Levine' theory.

The last development of this approach was made recently by Ohshima, Shilov and Dukhin [20,48,49]. We used Shilov–Zharkikh cell model for dynamic electrophoretic mobility. We call combination of O'Brien's relationship and our dynamic electrophoretic mobility theory the 'hybrid O'Brien's theory'.

For a time, it looked like O'Brien's approach had won out over the other approach because it appeared to yield a desirable electroacoustic theory for the concentrated case. However, one important question remains unsolved. In principle these two approaches must give the same result. It is not clear if it is the case. These two approaches are completely independent and relationship between them is not known even in dilute case. It is obvious that such comparison must be done. It would provide a strong support for O'Brien's theory if it confirms that two approaches merge. The first approach is somewhat more basic. It needs only major well tested electrokinetic equations.

The new theory based on the first approach has been created by A. Dukhin, V. Shilov, H. Ohshima and P. Goetz in the papers [13,50] for the simpler case of the CVI and/or CVP when gradient of pressure is a driving force generating electroacoustic signal. We would like to be cautious concerning expanding this new theory to the ESA phenomenon. It turned out that problem of frame of references has different implications for these different electroacoustic effects.

This new theory applies several assumptions. First, it is valid only for thin double layer

$$\kappa a \gg 1, \tag{43}$$

where κ is reciprocal Debye length. The first attempt to eliminate this restriction in electroacoustic theory has been described in the papers [58,59].

Second, it assumes surface conductivity κ^{σ} to be the same for all particles independently on their size.

Third, it considers frequency only below Maxwell–Wagner dispersion [51]:

$$\omega \ll \omega_e = \frac{K_m}{\varepsilon\varepsilon_0}, \tag{44}$$

where ε and ε_0 are dielectric permittivities of the medium and vacuum, K_m is the conductivity of the medium.

This improved electroacoustic theory yields the following expression for CVI:

$$\mathrm{CVI} = \frac{9\varepsilon\varepsilon_0\zeta(\rho_p - \rho_m)\nabla P}{4\eta} \frac{\sum_{i=1}^{N} (1/((Du_i + 1) - (Du_i - 0.5)\varphi))\,(\varphi_i h(\alpha_i)/\, j\alpha_i I(\alpha_i)(\rho_p - \rho_m(3H_i/2I_i + 1)))}{1 - (\rho_p/1 - \varphi)\sum_{i=1}^{N} \varphi_i(3H_i/2I_i + 1)/\rho_p - \rho_m(3H_i/2I_i + 1)}, \tag{45}$$

where a is a particle size, $\alpha = a\sqrt{\omega/2\nu}$, $\beta = b\alpha/a$, special functions h, H and I are given below, $H_i = H(\alpha_i)$, $I_i = I(\alpha_i)$ and

$$Du_i = \frac{\kappa^{\sigma}}{K_m a_i}. \tag{46}$$

This theory takes into account surface conductivity effects and as a result is valid for any value of the Dukhin number. This dimensionless parameter was introduced by Lyklema [6].

It turned out that there is contradiction between new electroacoustic theory and O'Brien's theory even modified with the new expression for dynamic mobility. Fig. 4 illustrates significance of the difference between two theories. Which one is correct?

There is an opportunity to answer this question using quasi-stationary limit of low frequencies. It is possible to derive an independent expression for CVI in this stationary case using Onsager relationship and Smoluchowski law. Comparison of both theories with this low frequency limit shows that the new theory (Eq. (45)) satisfies transition requirement to the stationary case whereas O'Brien theory does not.

This conclusion was proved experimentally in the paper [13].

Failure of the O'Brien's relationship to satisfy the Onsager principle and experiment is very unfortunate for electroacoustic theory because it prevents us to use a very convenient Eq. (42) and notion of dynamic electrophoretic mobility.

We would like to stress that according to our knowledge commercially available electroacoustic spectrometer based on ESA principle — Acoustosizer of Colloidal Dynamics, applies empirical correction for calculating ζ-potential from the ESA signal. It follows directly from the recent review published by Professor Hunter who is one of the Acoustosizer authors [12]. This correction is necessary because, as Professor Hunter admits, their theory is valid only up to 5 vol.%. This empirical correction works and reduces dramatically error of the Acoustosizer in some concentrated systems. Unfortunately, this empirical corrections mask results of theoretically justified calculations.

So far, the new electroacoustic theory has been tested with rigid heavy particles only. It is not clear yet how it will work for emulsions as there were no experimental data with emulsions available. This concern is related to the fact that this

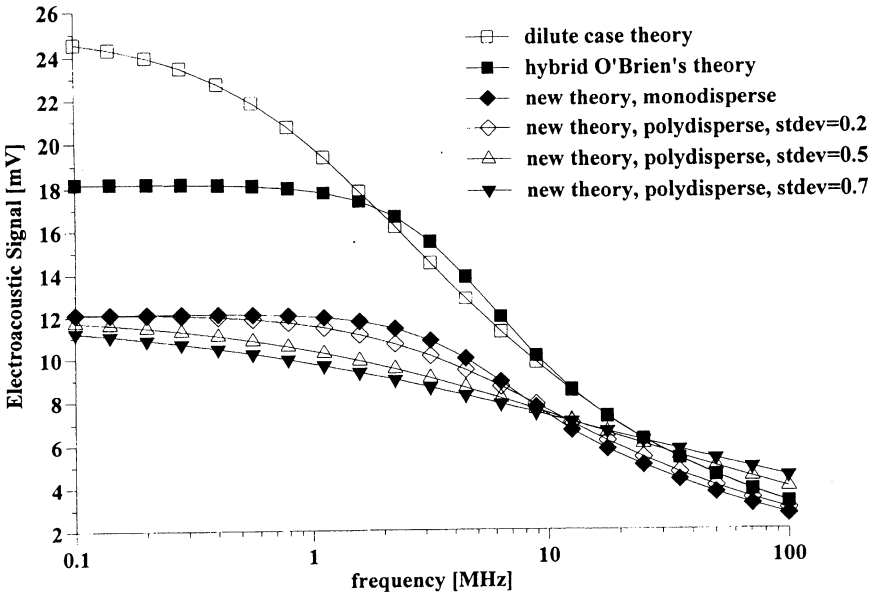

Fig. 4. Theoretically calculated normalized CVI (Eq. (22)) versus frequency for dispersion with 20 vol.% of 1 μ particles. Density of the liquid is 1 g cu^{-1} cm, of the particles-2 g cu^{-1} cm.

new theory as well as O'Brien's theory neglect thermodynamic effects. It is rather surprising as the thermodynamic effect of 'thermal losses' is dominant for acoustics of emulsions. It is not clear yet why electroacoustics is so different from acoustics for thermodynamic effects not to be important.

A simple hypothesis which might explain this difference is that electroacoustics is related to the displacement of the electric charges in the double layer (DL). This displacement is characterized by dipole symmetry ($E = f(r) \cos\theta$). At the same time 'thermal losses' measured by acoustics are associated mostly with spherical symmetry. They are caused by oscillation of the particle's volume in the sound wave. It is clear that such a spherical symmetrical oscillation does not necessarily cause displacement of electric charges with dipole structure.

This is a hypothesis, and a fundamental theory that will take into account the thermodynamic effects in addition to electrodynamic and hydrodynamic effects should resolve this question. The electroacoustic theory of emulsions will not be complete unless such a theory is developed.

Nevertheless, electroacoustics even at its present stage can yield very important information about electric surface properties of emulsions as will be shown below.

8. Electroacoustic ζ-potential probe

The new electroacoustic theory has been accompanied with the new device for measuring Colloid Vibration Current. It is ζ-potential probe DT-300 by Dispersion Technology Inc [53,54]. It consists of two parts: electronic part and sensor part.

All electronics are placed on two special purpose boards (Signal Processor and Interface). It requires also a conventional Data Acquisition card. The Signal Processor board and DAC are placed inside of a personal computer which performs interface with user using Windows based software.

The electroacoustic sensor probe contains a piezoelectric transducer with a critical frequency 3 MHz and a sensing electrode which is placed on the surface of the transducer. This electrode is separated from the external reference electrode with a non-conducting rigid ceramic insert. Internal electric impedance between these electrodes can be

selected depending on the conductivity range of the samples by means of an internal transformer. The transformer is selected such that the input impedance is significantly less than the external impedance of the sample such that the resultant signal is proportional to the short circuit current. This transformer is located just behind the central electrode in order to minimize the stray capacitance.

There is a special plastic rod between transmitting transducer and the sensing electrode with a low acoustic impedance. This rod adjust acoustic impedance of the probe and dispersion eliminating a high reflection on this surface. This additional rod opens a way to calibrate an absolute power using reflection on the transducer-rod surface.

The signal processor generates the transmit gate which defines the 1 Watt pulse generated in the Interface module as well as the necessary signals to set the frequency. Electroacoustic measurement can be performed either for one frequency or for the chosen set of frequencies from 1 to 100 MHz. Transducer converts these pulses to the sound pulses with some certain efficiency. Sound pulse propagates through the quartz delay rod, acoustic impedance rod and eventually through the sample. Acoustic pulse propagating through the sample excites particles, disturbs their double layers. Particles gain dipole moments because of this excitation. These dipole moments generate electric field. This electric field changes the electric potential of the central sensing electrode. Difference of the electric potentials between central electrode and external reference electrode causes electric current. This current is registered as Colloid Vibration Current. The value of this current is very low. It takes averaging of at least 800 pulses in order to achieve the high signal to noise ratio. Number of pulses depends on the properties of colloid. Measurement of CVI in low conducting oil based systems requires averaging of millions pulses. In principle, this method makes it possible to measure any low energy signals.

The general expression for the local CVI (Eq. (45)) contains one unknown parameter: P pressure. Pieso crystal converts initial 1 W electric signal to the sound with low efficiency, about 40 dB loss. The efficiency of this conversion is frequency dependent which makes additional problem for frequency CVI spectra measurement. Sound intensity after piesocrystal is rather low and not very well defined. Each pieso crystal has unique efficiency. Then, pulse propagate through the delay rod, acoustic impedance rod and partially reflects from the sensor–liquid surface. This changes amplitude of pressure again. As a result we do not know exact pressure at the point of the measurement.

Colloid vibration current can be presented in the simplified form:

$$\mathrm{CVI} = C*\zeta*\nabla P*G(\varphi, a)*Z_{\mathrm{dis}}/(Z_{\mathrm{dis}} + Z_{\mathrm{rod}}), \quad (47)$$

where C is a geometry calibration constant which characterizes complex distribution of the electric and sound fields near the electrodes surfaces, the multiplier with acoustic impedances of the dispersion Z and impedance rod Z characterizes reflection on the probe surface, function G is defined with Eq. (45).

Neither of the C and P are known. In order to exclude them we use calibration procedure described below.

In order to eliminate unknown constants C and P we use calibration with Ludox at 10% wt. diluted with KCl 10^{-2} mol l^{-1}. This silica particles have ζ-potential -38 mV at pH 9.3. CVI value for this colloidal silica can be expressed as following:

$$\mathrm{CVI}_{\mathrm{sil}} = C*\zeta_{\mathrm{sil}}*\nabla P*G(\varphi_{\mathrm{sil}}, a_{\mathrm{sil}})*Z_{\mathrm{dis.sil}}/(Z_{\mathrm{dis.sil}} + Z_{\mathrm{rod}}). \quad (48)$$

From this equation we can calculate unknown C and P and use them for calculating CVI for other samples:

$$\mathrm{CVI} = \mathrm{CVI}_{\mathrm{sil}}*\zeta/\zeta_{\mathrm{sil}}*G(\varphi, a)/G(\varphi_{\mathrm{sil}}, a_{\mathrm{sil}})*Z_{\mathrm{dis}} *(Z_{\mathrm{dis.sil}} + Z_{\mathrm{rod}})/(Z_{\mathrm{dis}} + Z_{\mathrm{rod}})Z_{\mathrm{dis.sil}}. \quad (49)$$

Expression Eq. (49) can be used for calculating either ζ-potential only from the magnitude of the CVI.

In addition DT-300 measures a phase of the CVI signal. This phase yields a particle size information. In the case of a single frequency this measurement provides only a mean particle size. In the case of the multiple frequencies the more detail information about particle size distribution

is available. However, according to our experience, acoustic spectroscopy is much more suitable for characterizing the particle size distribution [55].

9. Titration experiments

Electroacoustic ζ-potential probe offers a very simple and fast way to perform electrochemical characterization of the surface. Software of DT-300 has several optional titration protocols for running two burettes. These burettes are able to inject chemicals with increments as low as 0.2 μl.

The most common is pH titration. User should specify maximum and minimum pH, number of points, number of sweeps, direction. This software assumes 1 N acid and base. In addition user can change equilibration time, tolerance, sample volume, etc.

Equilibration time is very important parameter. Titration makes sense only if it follows the equilibrium root. Some systems exhibit a very long equilibration time. The good example is a concentrated zirconia dispersion. Fig. 5 shows evolution of the ζ-potential and pH of the 3 vol.% zirconia dispersion in time. It is seen that equilibration time is about 30 min. For comparison, silica Ludox reaches equilibrium in a fraction of minute. A typical equilibrium titration of the silica Ludox at 10 wt.% is shown on Fig. 6. It is clear that it is almost impossible to make a similar equilibrium titration for zirconia because it takes a lot of time.

There is another type of titration when user adds a certain amount of reagent with a certain increment. It is called 'ml protocol' in the DT software. User specifies a total amount of the injected substance and number of points. Burette automatically inject this substance, wait the specified equilibration time and then CVI sensor measures ζ-potential. In addition DT-300 monitors pH and temperature continuously. A typical titration of this kind is shown on Fig. 7. It has been made using hexametaphosphate with precipitated calcium carbonate at 3 vol.%.

The most complicated problem for titrating concentrated dispersions is mixing. Mixing is absolutely necessary for the successful titration. However, it becomes hard to mix especially in the ranges of instability.

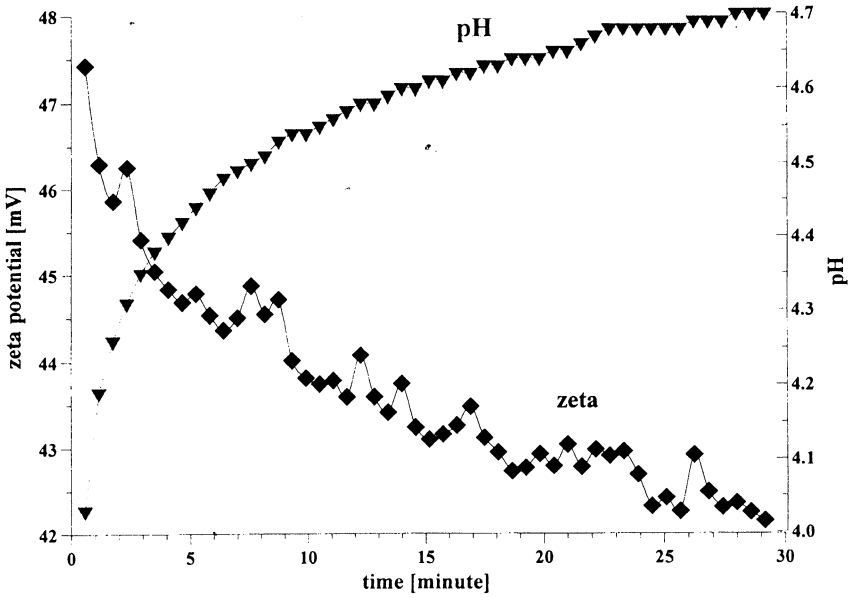

Fig. 5. Equlibration of 3 vol.% zirconia slurry prepared in the KCl 10^{-2} with pH adjusted initially to 4. It is seen that equlibration takes about 2 h.

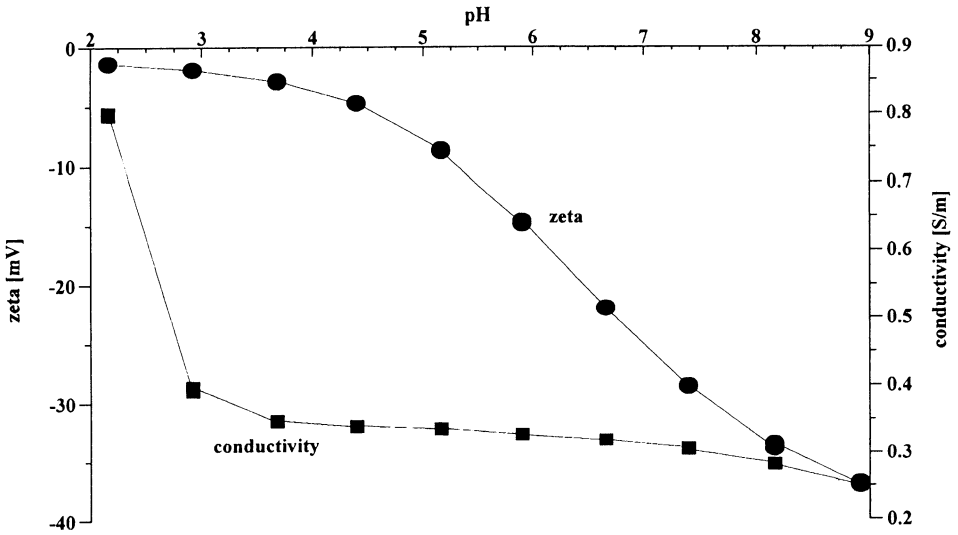

Fig. 6. Titration of the 10 wt.% silica Ludox using 1 N HCl and KOH.

We know only one solution of this problem: pumping sample through the measuring chamber. Traditional propeller mixers do not work with the paste like samples. Pumping makes it possible to involve a complete sample whereas propeller perform mixing only its own vicinity. Pumping functions properly only when measuring chamber does not have hydrodynamically stagnated spaces. Otherwise, deposit built up in these spaces can interrupt the flow.

We show here results of the titration performed with several kaolin slurries. These data has been published in the paper [56].

The kaolin used in this study was obtained from the Engelhard Corporation and was categorized as a fine grade crude with high iron content. Kaolin, in general, is defined by platelet crystals in which one of the dominant faces is made up of octahedral alumina and the other consists of tetrahedral silica. Particle aggregation thereby occurs when the negative platelet faces (negative due to isomorphic substitutions) interact with positive charge sites on the crystal edges (due to pH sensitive aluminol and silanol sites). The two dispersants used to study this aggregation phenomena were both common to the kaolin industry and consisted of 2.0 modulus silicate (Occidental Chemical Corporation) and sodium hexametaphosphate, SHMP (Albright and Wilson Americas Inc.). The 2.0 modulus being in reference to the average distribution of silicate species present (linear dimer, 3-D dimer and trimer). The 2.0 modulus silicate was expected to interact with the positive edge sites of the kaolin platelet through electrostatic interactions. The SHMP was a cyclic polyphosphate, which is expected to adsorb to the positive charges along the kaolin edges through both electrostatic and covalent bonding.

Titration of the kaolin EC1 slurry with hexametaphosphate reviled a strong pH dependence. Titration curve shifts depending on the initial pH value. It is illustrated on Fig. 8 for both ζ-potential and pH. It is not surprising because pH is a strong charge factor for kaolin. For instance, Fig. 9 presents pH titration of the 40 wt.% EC2 kaolin slurry. It is clear that ζ-potential goes up with pH.

Titration of EC1 kaolin slurry is a good example showing importance of various factors, not only dispersant concentration. It is convenient to illustrate this complex titration using 3-dimensional fingerprint. Fig. 10 shows this fingerprint for kaolin EC1 titration.

Titration of EC1 slurry illustrates existence of the optimum concentration of dispersant. One can see that increase of the hexametaphosphate concentration leads eventually to decreasing of ζ-po-

tential. In this particular case it is related to the increasing ionic strength and collapsing double layer.

Dependence of ζ-potential on pH is an additional factor which might be exploited for reaching higher ζ-potential values. From this viewpoint hexametaphosphate has disadvantage because it reduces pH. Another dispersant, silicate, is more advantageous from the pH viewpoint because its addition to the slurry increases pH, as it is shown on Fig. 11. However, even combined silicate-pH effect is not sufficient to gain ζ-potential values created with hexametaphosphate. Maximum value for silicate titration is -28 mV whereas hexametaphosphate yields -34 mV at maximum.

Hexametaphosphate is more efficient in terms of optimum amount as well. The maximum value of ζ-potential can be reached adding twice less hexametaphosphate (0.6% by kaolin weight) than silicate (1.3% by kaolin weight).

There is one more factor which affects stability of the kaolin dispersions: it is sonication. Apparently neither of tested chemical factors (pH, hexametaphosphate, silicate) destroys initial aggregates. These chemical factors create environment which is potentially beneficial for gaining a full stability, but in order to take advantage of this environment one should apply a strong agitation which would destroy aggregates. It turned out that just mixing does not help. Only powerful sonication is able to break aggregates. This effect is illustrated on Fig. 12. It is seen that sonication causes a large 5 mV jump in ζ-potential value. Actually it is somewhat misleading. Sonication does not affect surface charge. It creates a new surface and reduces particle size. Appearance of the new surface with the same ζ-potential leads to the larger CVI signal. This larger CVI signal can be interpreted as larger ζ-potential if we keep the same particle size. So far particle size was assumed to be 300 nm for all EC1 kaolin slurries.

There is an opportunity to prove independently that sonication affects particle size distribution. In order to do this we can use Acoustic measurement which is a part of DT-1200. This acoustic sensor measures attenuation of ultrasound. Attenuation spectra contains information about particle size. There are many examples of successful particle sizing using acoustics [55].

Fig. 13 shows attenuation spectra measured for various kaolin EC1 slurries. Slurries with hexametaphosphate and silicate are prepared at the optimum dispersant concentrations. Corresponding median sizes are given in the Table 3. It is seen that the smallest size can be reached with hexametaphosphate after applying sonication. This conclusion confirms our observations made with electroacoustic measurement.

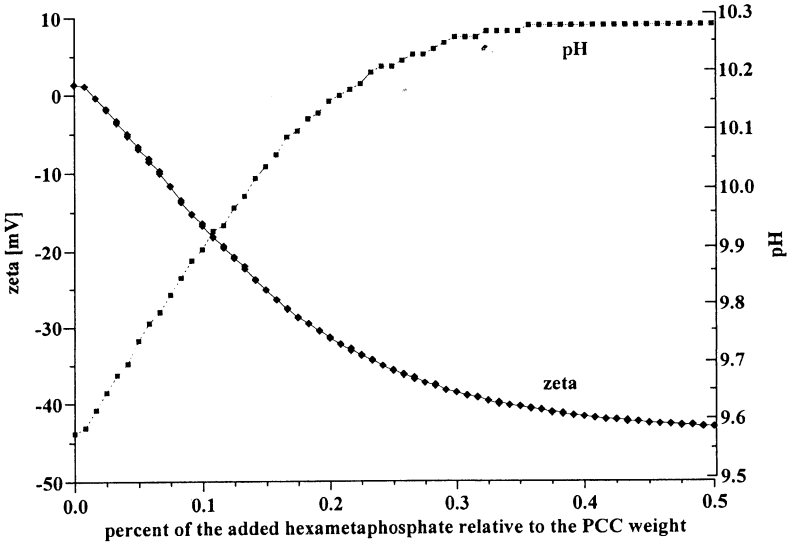

Fig. 7. Titration of the 3 vol.% PCC slurry with 0.1 g g^{-1} hexametaphosphate solution.

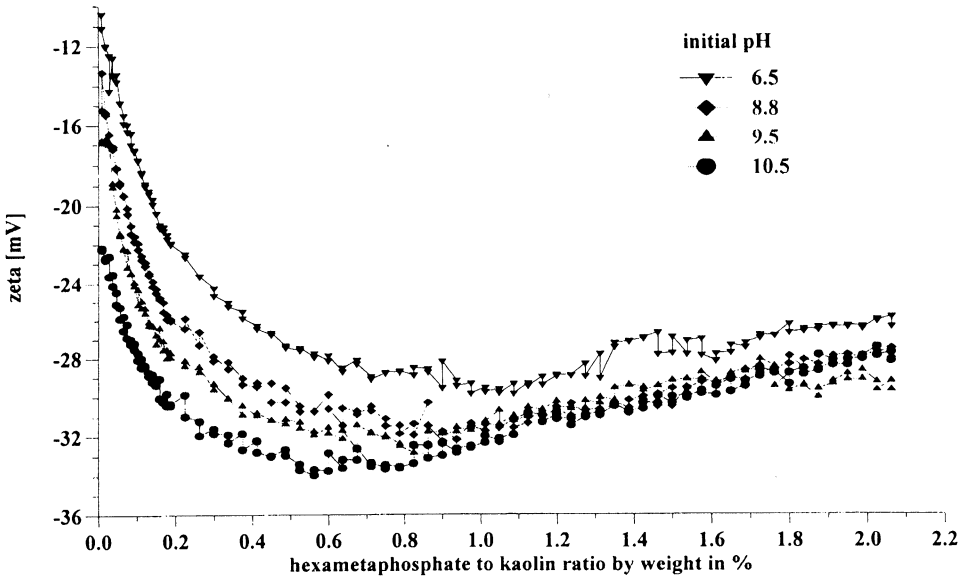

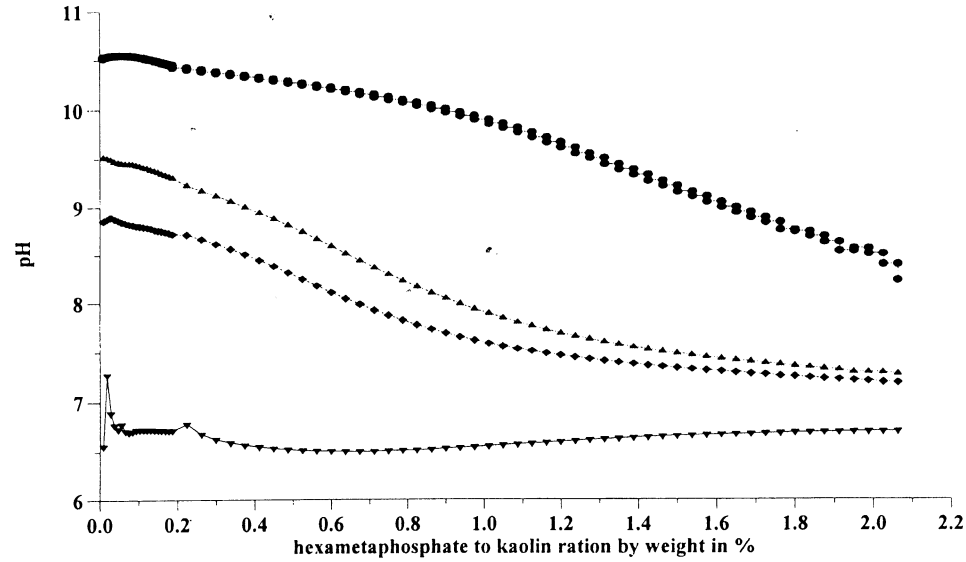

Fig. 8. Titration of the 40 wt.% kaolin EC1 slurry using hexametaphospate.

10. Mixed dispersions

There are many important natural and man-made dispersed systems containing a high concentration of more than one dispersed phase. For instance, whole blood contains many different types of cells, paint usually consists of latex with added pigment to provide color, and sunscreen

preparations include both an emulsion as well as sun-absorbing particles. In many such systems there is a practical need to determine the particle size distribution (PSD) of one or more ingredients. In general, light-based techniques are not well suited to provide this information because most optical methods require the sample to be diluted prior to measurement, thereby distorting or destroying altogether the particle size information being sought. Furthermore, most light-based systems cannot handle multiple disperse phases, even in the most dilute case. In contrast, acoustic attenuation spectroscopy [4,55,60–64] opens an opportunity to eliminate this undesirable dilution step.

There are at least three quite different philosophical approaches for interpreting these acoustic spectra.

In the simplest 'empirical' approach, we forego any size analysis per se and simply observe the measured acoustic attenuation spectra to learn whether, for example, the sample changes with time or if 'good' or 'bad' samples differ in some significant respect. Importantly, this empirical approach provides useful engineering solutions even in cases where we know nothing about the physical properties of the sample or whether indeed the sample is adequately described by our theoretical model.

In a more subtle 'validation' approach we assume in advance that we know the correct particle size distribution, and furthermore assume the real dispersion conforms to some model. We then use some predictive theory based on this model, as well as the assumed size distribution, to test whether this predicted attenuation matches that actually measured. If the validation fails, it is a very strong indication that the model is inadequate to describe the system at hand.

As an example of this validation approach, consider the case where we construct a mixed system by simply blending two single component slurries. The PSD of each single-component slurry can be measured prior to blending the mixed system. Since we have control of the blending operation we know precisely how much of each

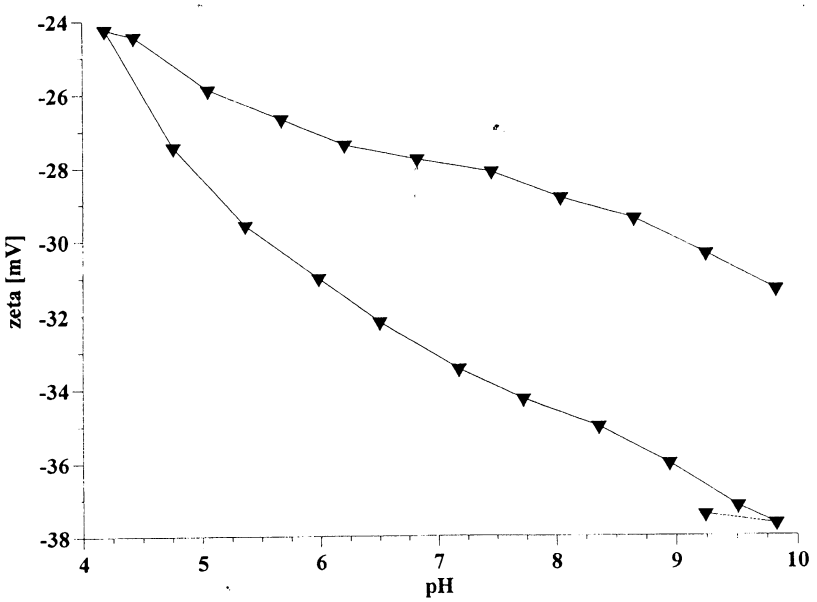

Fig. 9. pH titration of the 40 wt.% EC2 kaolin slurry.

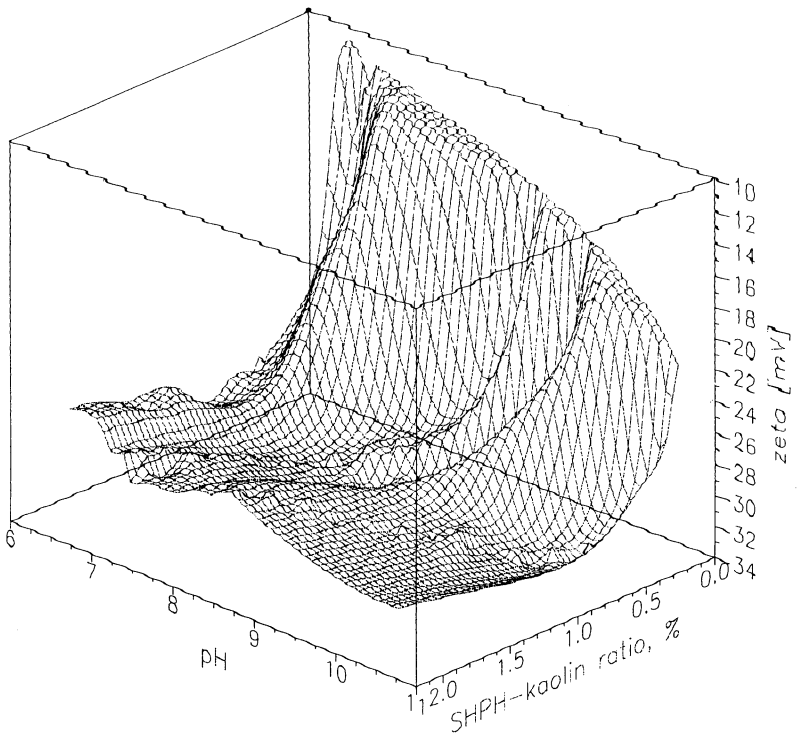

Fig. 10. Titration ζ-pH-hexametaphosphate fingerprint of the 40 wt.% kaolin EC1 slurry.

component is added. If we claim that the combined PSD is simply a weighted average of the individual PSD for each component, we are in effect assuming that there is no interaction between these components. In this case the prediction theory allows us to compute the theoretical attenuation for this mixed system. If the experimental attenuation spectrum matches the predicted spectrum then the assumption that the particles did not interact is confirmed. However, if the match is poor, it is then likely that the mixing of the two components caused some changes in the aggregative behavior of the system. Perhaps new composite particles were formed by some interaction of the two species. Or perhaps some chemical component in one sample interacted with the surface of another. Many interaction possibilities exist. Nevertheless, it seems appropriate to conclude that a necessary condition to rule out aggregation on mixing is that the experimental and predicted attenuation curves match. In addition we can probably also conclude that an error between theory and experiment is sufficient to say that some form of aggregation or dis-aggregation on mixing has occurred. We will show that such prediction arguments are indeed able to monitor such aggregation phenomena.

Finally, we can take the ultimate leap and use an 'analysis' algorithm to search for that particle size distribution which in accordance with the model and the predictive theory best matches the experimental data.

Importantly, both the 'validation' and 'analysis' approach assume that we can accurately model the real world, while at the same time making some simplifying assumptions. For example, it is common to assume that the particles can be treated as spheres, even though we know that this may not be exactly the case. Here, we follow the paper [57] which suggests two models that can be particularly helpful for describing mixed dispersions.

The first 'multi-phase' model assumes that we can represent the PSD of a real-world dispersion

as a sum of separate lognormal distributions, one for each component in the mixed system. For this paper we assume that there are only two components, which reduces the overall PSD to a simple bimodal distribution. When we calculate the attenuation of such a multi-phase system we take into account the individual density and other particles properties for each component in the mixture. For a bimodal case, the multi-phase approach would typically require the analysis algorithm to fit five adjustable parameters: the median size and standard deviation of both modes and the relative mass fraction of each mode. In this work we will assume that the weight fraction of each mode is known in advance. Furthermore, in an effort to avoid the well-known problem of multiple solutions, we will further assume that both modes have the same standard deviation. Altogether, these simplifications reduce the number of adjustable parameters to just three: the median size of each mode and the standard deviation. The implications of these simplifications will be discussed later.

The second 'effective medium' model further assumes that one needs to determine the PSD of just one component in an otherwise complex mixed system. All other disperse phases are lumped together into an effective homogeneous medium characterized by some composite density, viscosity and acoustic parameters. By adopting this viewpoint, we significantly reduce a complex real-world mixture to a simpler dispersion of a single pre-selected dispersed phase in a newly defined 'effective medium'. We need not even define the exact nature and composition of this new medium since we can simply measure, or perhaps calculate, the required composite density, viscosity, attenuation and sound speed. If we assume that the key disperse phase can be described by a lognormal distribution then we have reduced the degree of freedom to just two adjustable parameters, a median size and standard deviation.

In the paper, we have evaluated the effectiveness of both the multi-phase and the effective medium model using the same set of experimental data. As a result we gain a better understanding of the restrictions and benefits of each method.

We used three pigments from Sumitomo Corporation: AKP-30 alumina (nominal size 0.3 μ), AA-2 alumina (2 μ) and TZ-3YS zirconia (0.3 μ). In addition we used precipitated calcium carbonate (PCC) supplied by Specialty Minerals Corp. (0.7 μ) and Geltech silica (1 μ).

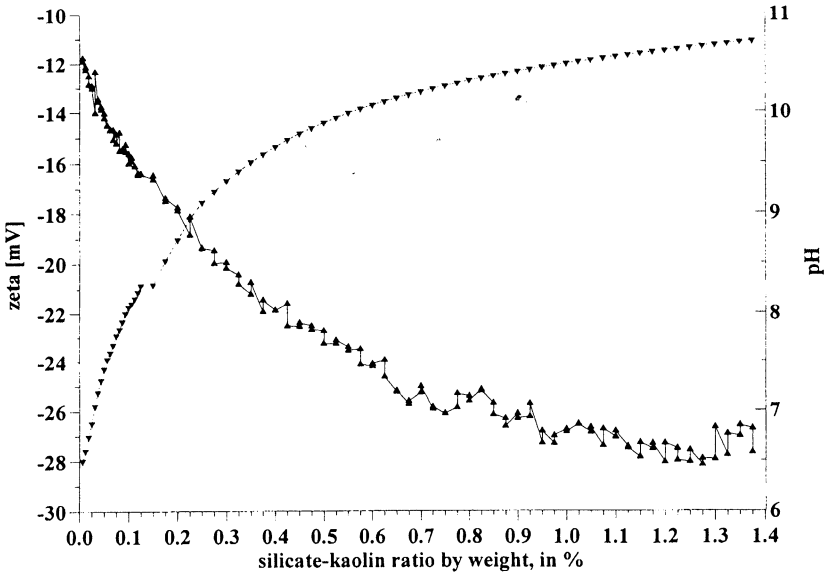

Fig. 11. Titration of 40 wt.% EC1 kaolin slurry using silicate.

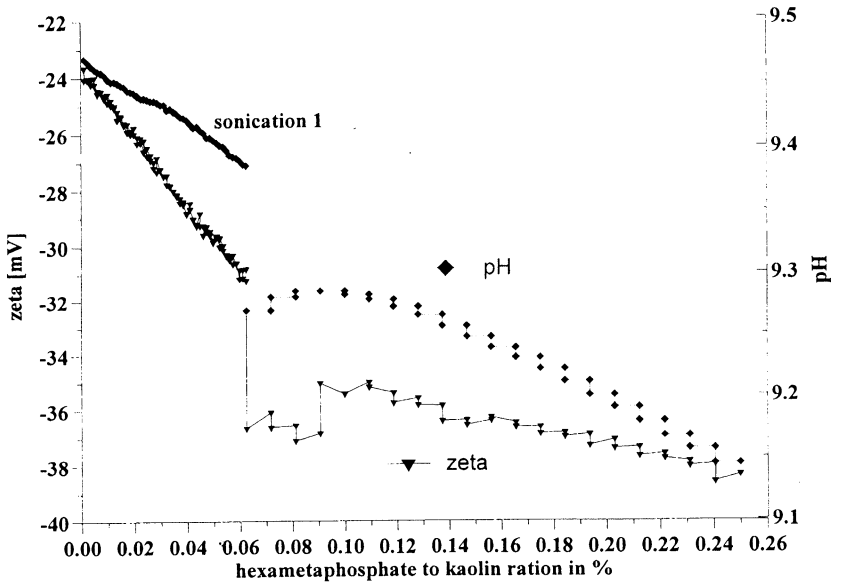

Fig. 12. Effect of sonication on the EC1 40 wt.% kaolin titration with hexametaphosphate.

Slurries of the AA-2 alumina, and the zirconia were prepared in such a manner as to have quite good aggregative stability. Each slurry was prepared at 3 vol.% by adding the powder to a 10^{-2} mol l^{-1} KCl solution, adjusted initially to pH 4 in order to provide a significant ζ-potential. Although the alumina showed very quick equilibration, the zirconia required about 2 h for the zeta potential and pH to equilibrate as shown in Fig. 5. Both slurries were judged to be quite stable under these conditions as indicated by the absence of any noticeable settling.

Preparation of a 3 vol.% PCC slurry was more problematic since the ζ-potential right after dispergating was very low (1.3 mV). Control of pH alone was insufficient and we therefore used sodium hexametaphosphate in order to increase the surface charge and improve the aggregative stability of this slurry. In order to determine the optimum dose we ran a ζ-potential titration, the results of which are shown in Fig. 7. The ζ-potential reaches saturation at a hexametaphosphate concentration of about 0.5% by weight relative to the weight of the PCC solid phase.

The Geltech silica and the AKP-30 alumina were used only as dry powders, being added to the PCC slurry as needed.

The goals of the experiment were met in the following steps:

Step 1: Three single component slurries of alumina AA-2, zirconia and PCC respectively, were prepared as described above.

Step 2: The attenuation spectra of these single component slurries were measured and the particle size distribution for each was calculated.

Step 3: Three mixed alumina/zirconia slurries were prepared by blending the above slurries in different proportions and the attenuation spectra for each mixture was measured.

Step 4: Geltech silica powder was added to the initial PCC slurry and the attenuation spectra was measured for this mixed system.

Step 5: AKP-30 alumina powder was added to the initial PCC slurry and the attenuation spectra for this mixed system was measured.

Step 6: The particle size distribution was calculated for all of the mixed systems using the 'multiphases model'.

Step 7: The properties of the 'effective medium' were calculated for all mixtures.

Step 8: The particle size distribution for each of these mixed systems was calculated using the 'effective medium model'.

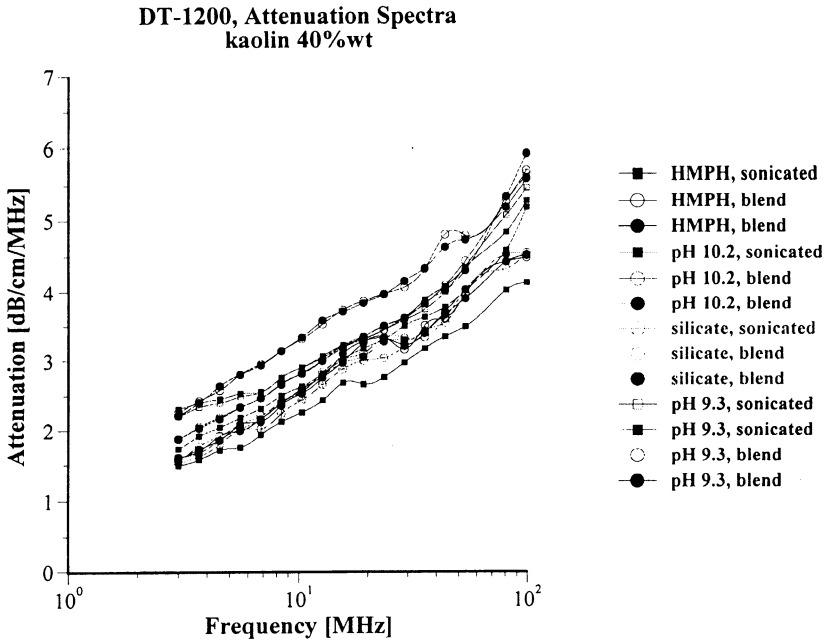

Fig. 13. Attenuation spectra measured for EC1 40 wt.% kaolin slurry stabilized either with pH, or hexametaphoshate, or silicate.

Step 9: The results of the particle size calculation using two different approaches were compared.

Step 10: The validation approach was used to test for possible particle interactions in the mixed systems.

The experimental attenuation spectra for the three single component slurries and five mixtures are shown in Figs. 14 and 15. In order to demonstrate reproducibility, each sample shown in Fig. 14 was measured at least three times. Mixture 1, in fact was measured yet a fourth time after a fresh sample was loaded just to show that sample handling was not a factor. It is clear that the reproducibility is sufficient for resolving the relatively large differences in attenuation between different samples.

The attenuation spectrum for the single component slurries of the AA-2 alumina, the zirconia and the PCC allows us to calculate the particle size distribution for each of these materials. The calculated sizes are given in the Tables 4 and 5 and it is seen that these acoustically defined sizes agree quite well with the nominal sizes given by the producers of these materials.

As shown in Figs. 14 and 15, the attenuation spectra of the mixtures differ significantly from the attenuation spectra of the single component slurries. This difference in the attenuation spectra reflects the differences in both the particle size distributions and the density of the constituent components in the mixtures.

Table 3
Median particle size calculated from slurry

Chemical name	Median log
Hexa, sonicated	0.2122
Hexa, blend	0.2621
Hexa, blend	0.2621
pH 10.2, sonicated	0.2658
pH 10.2, blend	0.3002
pH 10.2, blend	0.2978
pH 10.2, blend	0.3017
Silicate, sonicated	0.2362
Silicate, blend	0.2627
Silicate, blend	0.2586
pH 9.3, sonicated	0.3063
pH 9.3, blending	0.3671
pH 9.3, blending	0.366

Table 4
Characteristics of alumina AA-2 and zirconia TZ-3YS slurries and their mixtures

	Initial		Mixture 1		Mixture 2		Mixture 3	
	Alumina	Zirconia	Alumina	Zirconia	Alumina	Zirconia	Alumina	Zirconia
Volume fraction,%	3	3	1.55	1.45	1.85	1.15	2.28	0.72
Weight fraction,%	10.96	15.91	5.5	7.9	6.6	6.3	8.2	4
Effective viscosity [cp]			0.92		0.93		0.94	
Effective density [g cm^{-3}]			1.04		1.05		1.06	
att $M0$	1.593		1.21		0.982		0.823	
att $M1$	0.0845		0.0642		0.0521		0.0437	
att $M2$	−1.251		−0.95		−0.771		−0.646	
att $M3$	0.528		0.401		0.326		0.273	
Parameters of the particle size distributions, effective medium approach								
Median lognormal [micron]	2.15 ± 0.02	0.33 ± 0.006		0.293 ± 0.006		0.303 ± 0.005		0.317 ± 0.003
SD	0.26	0.43		0.38		0.378		0.372
Fitting error,%	6.6	1.9		1.4		1.2		0.95
Parameters of the particle size distributions, two dispersed phases approach								
Median size [micron]			0.565 ± 0.002	0.558 ± 0.001	2.922 ± 0.088	0.352 ± 0.005	3.582 ± 0.182	0.303 ± 0.003
SD			0.53		0.3		0.21	
Fitting error,%			5		7.6		4.4	

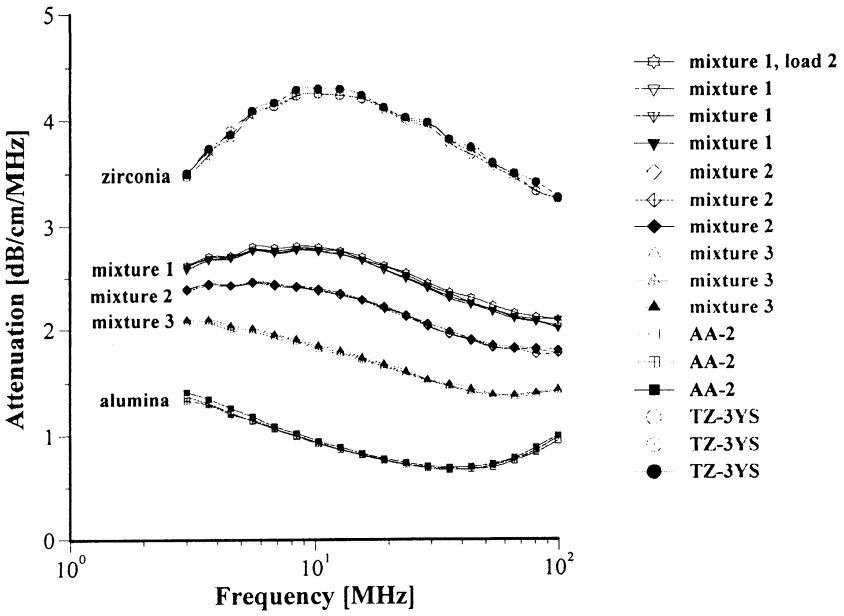

Fig. 14. Experimental attenuation spectra for initial alumina AA-2 and zirconia TZ-3YS from Sumitomo and their mixtures with weight fractions given in the Table 4. This figure illustrates reproducibility, including two loads for the mixture 1.

We want to compare the effectiveness of the 'multi-phase' and the 'effective medium' approach in calculating the PSD of these five different mixed systems.

First let us consider the more or less straightforward 'multi-phase' model. To use this approach we need only know the weight fraction and density of both disperse materials. The present software implementation assumes that the total particle size distribution is bimodal and that each mode corresponds to one disperse phase material. For instance in the alumina/zirconia mixture the smaller mode corresponds to the zirconia and the larger mode corresponds to the alumina. The software takes into account the difference in densities between materials of the first and the second modes. The PSD of each mode is itself assumed to be lognormal. In order to reduce the number of adjustable parameters, and in an effort to reduce the likelihood of multiple solutions, the present software implementation assumes that both modes have the same standard deviation. The software searches for some combination of three adjustable parameter (two median sizes and their common standard deviation) that provide the best fit to the experimental attenuation spectra. It assumes the relative content of the modes to be known.

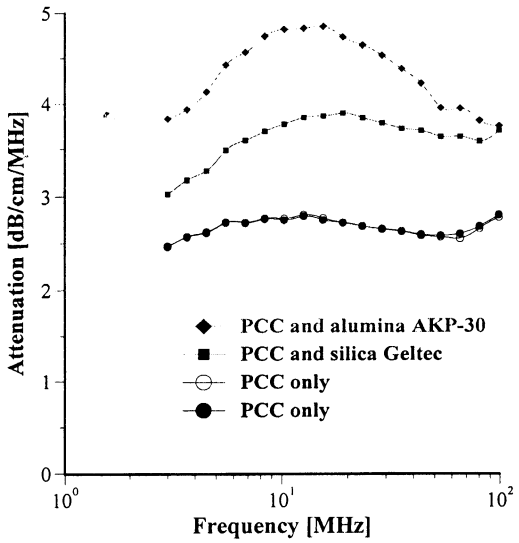

Fig. 15. Experimental attenuation spectra for initial PCC slurry and its mixture with the added silica and alumina powders. Weight fractions are given in the Table 5.

Table 5
Characteristics of PCC slurry and its mixtures with alumina AKP-30 and silica Geltech

	Initial PCC	Initial silica	PCC and silica		PCC and alumina	
		Powder	PCC	Silica	PCC	Alumina
Volume fraction,%	10.55		9.19	6.29	10.27	2.52
Weight fraction,%	23.53		19.6	11.3	21.6	8.1
Effective viscosity [cp]	1.125		1.094		1.118	
Effective density [g cm^{-3}]	1.17		1.13		1.15	
att $M0$	1.053					
att $M1$	4.431					
att $M2$	−3.648					
att $M3$	0.9296					
Parameters of the particle size distributions, effective medium approach						
Median lognormal [micron]	0.684	1.26		0.454		0.325
SD	0.31	0.35		0.015		0.015
Fitting error,%	1.1	1.3		7.5		2.4
parameters of the particle size distributions, two dispersed phases approach						
Median size [micron]			0.449	0.681	0.798	0.2715
SD			0.16		0.19	
Fitting error,%			8		1.9	

The corresponding PSD for these five mixed systems are shown in Figs. 16 and 17. The parameters of these PSD are given in Tables 4 and 5. It is seen that in some cases this 'multi-phase' approach yields approximately the correct size. For instance, the two zirconia/alumina mixtures with a lower zirconia content (mixtures 2 and 3) have almost the correct size combination. The size of the alumina particles is somewhat higher than expected (2.15 μ) but is still rather acceptable. We can say the same about the PCC/alumina mixture from Table 5. The difference of the sizes relative to the nominal values does not exceed 10%.

However, the multi-phase model appears a complete failure for the alumina/zirconia mixture 1 as well as the PCC/silica mixture. It is not clear yet why this 'multi-phases model' works for some systems and not for others. We think it probably is related to the fact that the present software assumes that both particle size modes have the same width. It is seen that the single component zirconia slurry has a PSD that is much broader (SD = 0.43) than the PSD of the AA-2 alumina (SD = 0.26). The bimodal searching routine finds the correct intermediate value for the standard deviation (0.3) only for mixture 2. It is interesting that this PSD solution is the closest match to the superposition of the initial PSD. The standard deviations for the other two mixtures are out of range completely and the corresponding PSD also deviate from the expected superposition.

This observation allows us to conclude that our restriction that the standard deviation be the same for both modes might itself create an artificially wrong solution. It is easy to eliminate this restriction but as one adds additional degrees of freedom it is not uncommon to be faced with the problem of multiple solutions.

This multiple solution problem appears when the error function (difference between experimental and theoretical attenuations) has several local minimums with different combinations of the adjustable parameters. In general, the problem of multiple solutions increases as the number of adjustable parameters increases. It seems clear that the maximum number of adjustable parameters to avoid multiple solutions is not a fixed number but

rather depends on a combination of factors: the accuracy and amount of experimental data points, the degree to which the real world sample is described by the model, and how accurately the key parameters of the colloid such as weight fraction, density, etc are known. Our experience is that bimodal PSD with even four adjustable parameters sometimes exhibit multiple solutions. We have found ways to resolve these multiple solutions in the case of single component dispersions, however the situation is more complicated for mixed dispersions with two or more chemically different components. For this reason, we restricted the number of the adjustable parameters to only three for this work.

These results indicate that the 'multi-phase' model might sometimes lead to wrong solutions and it is unclear at this point how to completely eliminate the problem.

In contrast, the 'effective medium' approach circumvents this problem by addressing only the question of determining a simple lognormal distribution that describes only one disperse phase in an otherwise complex mixture. Since we are then dealing only with two adjustable parameters (median size and standard deviation) the possibility for multiple solutions is most likely diminished. On the downside, when using the 'effective medium' approach we need to perform an additional experiment to measure the properties of this 'effective medium' and this may not always be possible or without other difficulties.

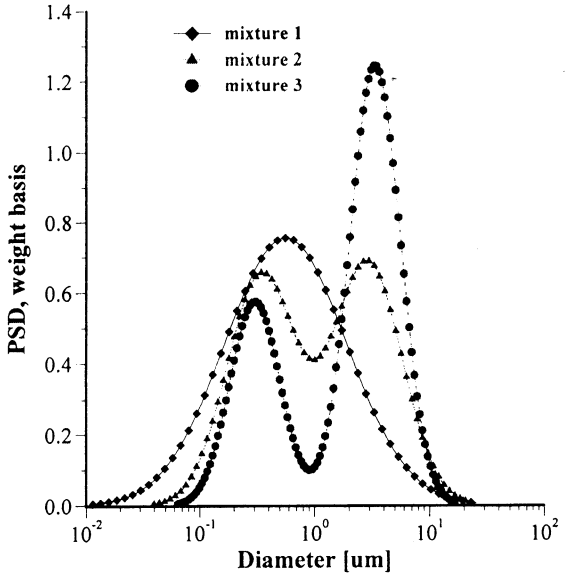

Fig. 16. Particle size distributions calculated for alumina–zirconia mixtures using 'multi-phases model'. The smaller size mode corresponds to zirconia, the larger size mode is alumina AA-2. Weight fraction and PSD parameters are given in the Table 4.

In the case of the PCC mixtures with the added alumina or silica, the original PCC slurry itself serves as the 'effective medium'. We need just three parameters to characterize this 'effective medium' namely: density, viscosity and attenuation. Importantly, all three parameters can be directly measured if we have access to this medium. The attenuation is the most important of these three required parameters. It is also the most challenging to characterize because we need the attenuation of this medium as a function of frequency from 3 to 100 MHz. The current version of the DT 1200 software allows us to define the attenuation of the effective medium the same way we would normally define the 'intrinsic attenuation' of even a pure liquid medium. This intrinsic attenuation as measured in dB cm^{-1} per MHz can be described in terms of a polynomial function:

$$\mathrm{att}(f) = \mathrm{att}\ M0 + f\,\mathrm{att}\ M1 + f^2\,\mathrm{att}\ M2 + f^3\,\mathrm{att}\ M3,$$

where f is frequency in MHz, and $M0$, $M1$, $M2$ and $M3$ are the polynomial coefficients.

For example, in the simplest case we can say that our effective medium is just water. Water has an attenuation that for practical purposes can be said to simply increase as a linear function of frequency if attenuation is expressed in dB cm^{-1} per MHz. Thus $M0$, $M1$, $M2$ and $M3$ are zero and $M2$ represents this linear dependence.

To use the effective medium approach for mixed systems, we simply need to define new coefficients to describe the intrinsic attenuation of this new medium. In the case of the alumina/zirconia mixtures we use the alumina slurry as the 'effective medium'. The coefficients for the alumina slurry can be calculated by doing a polyno-

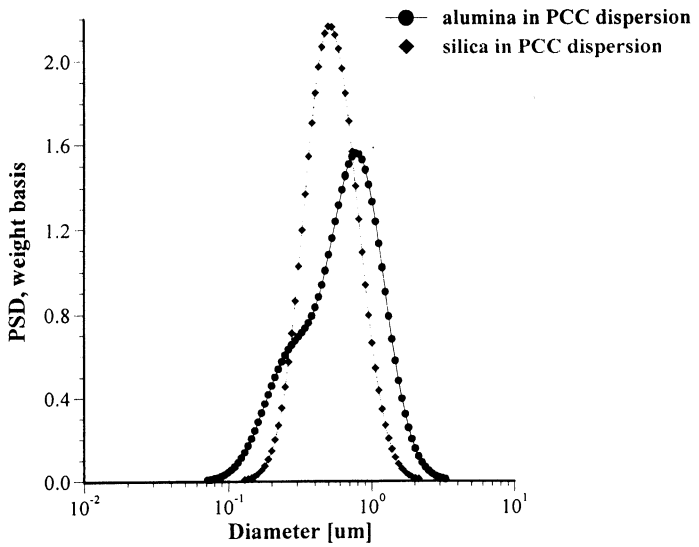

Fig. 17. Particle size distributions calculated for PCC–alumina and PCC–silica mixtures using 'multi-phases model'. Weight fraction and PSD parameters are given in the Table 5.

mial fit to the attenuation data as shown in Fig. 18(A). These coefficients are also given in Table 4. Similarly, the coefficients for the PCC 'effective medium' can be calculated from a polynomial fit of the attenuation data for that material as shown in Fig. 18(B). Likewise, these coefficients are given in Table 5.

We should keep in mind that the initial alumina slurry is diluted when we mix it with increasing amounts of the zirconia slurry. As a result, we need to recalculate the attenuation coefficients for each mixture taking into account the reduced volume fraction of the alumina in each mixture. The suitably modified values for the attenuation coefficients of the effective medium for all three alumina/zirconia slurries are also given in the Table 4. We avoided the need for making these additional calculations in the case of the PCC mixtures by simply adding dry silica or alumina powder to the PCC effective medium, and therefore the coefficients for the PCC effective medium is the same for both mixtures.

For an aqueous medium, the software automatically calculates the intrinsic attenuation of water and subtracts this from the measured attenuation to deduce the attenuation caused solely by the presence of the disperse particles. When using the 'effective medium' model, the software actually works in the same way, except that the intrinsic attenuation of water is replaced by the attenuation of this new effective medium. For instance, in the case of the PCC/alumina mixture the software calculates the attenuation due to the PCC contribution and subtracts it from the total attenuation of the mixture. The residual part corresponds to the attenuation due to the alumina particles and is the source of the particle size information for the alumina component. The software assumes a log-normal PSD and fits this residual attenuation using the median size and standard deviation as adjustable parameters.

This effective medium approach allows us to calculate the particle size distribution of the zirconia in the alumina/zirconia mixtures and of the silica or the alumina in the case of PCC mixtures. The corresponding values are shown in Tables 4 and 5. Figs. 19 and 20 illustrate the corresponding PSD for each case.

In the case of zirconia we have almost the same PSD for all three mixtures. This PSD agrees well with the initial slurry. The fitting error is much smaller than in the 'multi-phase model' which is an additional indication of the consistency.

In the case of PCC mixtures the situation is more complicated. We have a very good correlation with the nominal size for the AKP-30 alumina for PCC-alumina mixture with a good fitting error.

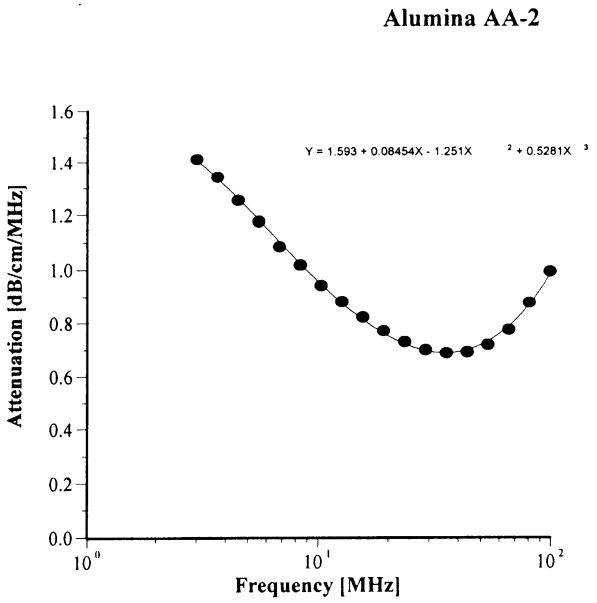

Fig. 18. Experimental attenuation spectra measured for individual alumina AA-2 slurry and PCC slurry with polynomial fit.

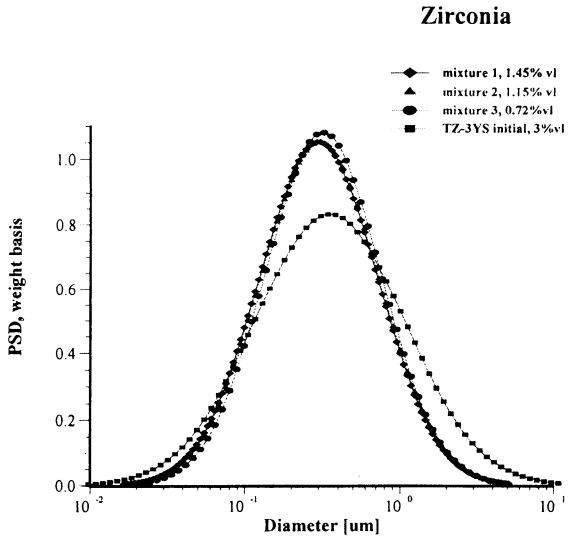

Fig. 19. Particle size distribution calculated using 'effective medium model'. The case of zirconia in the alumina AA-2 dispersion as the effective medium. Attenuation of the alumina is reduced according to volume fractions from the Table 4. Density and viscosity are adjusted as effective medium.

The other PCC based mixture gives a particle size which is twice smaller than expected. You can see from the Table 5 that the calculated size of the silica Geltech is only 0.454 μ whereas the nominal size is at least 1 μ. We measured acoustically for this silica even larger size of 1.26 μ. It might happen because of the dispersing problems. We have found that this silica is difficult to disperse properly even at high pH and high zeta potential. For instance, we measure ζ-potential of -66 mV for this silica at pH 11 but even this was apparently not sufficient to disperse it completely.

Summarizing the Analysis results for these five mixtures, we conclude that in the case of the three mixed dispersions (alumina–zirconia mixtures 2 and 3, and the PCC–alumina mixture), the 'multiphase model' and the 'effective medium model' gave similar results and reasonable PSD. For the other two mixtures, the results are more confusing. We suspect that the failure of the 'multiphases model' for the alumina–zirconia mixture 1 is related to the restriction on the PSD width, but

particles aggregation is still a candidate as well. In the case of the PCC–silica mixture a double failure of the both modes certainly point towards particle aggregation.

We can evaluate these ideas about aggregation of the two troubled mixtures using the 'validation' approach. To do this we must first compute the total PSD using the known PSD of the individual single component dispersions. Next, we calculate the predicted attenuation for this combined PSD. This predicted attenuation should agree with the experimental spectrum for the mixed system if there is no particle interaction between the species.

Fig. 21 illustrates the predicted and experimental attenuation spectrum for the Zirconia–alumina mixture 1 and the PCC–silica Geltech mixture. For both mixtures we have also added the predicted attenuation corresponding to the best PSD calculated using the 'multi-phase model' analysis.

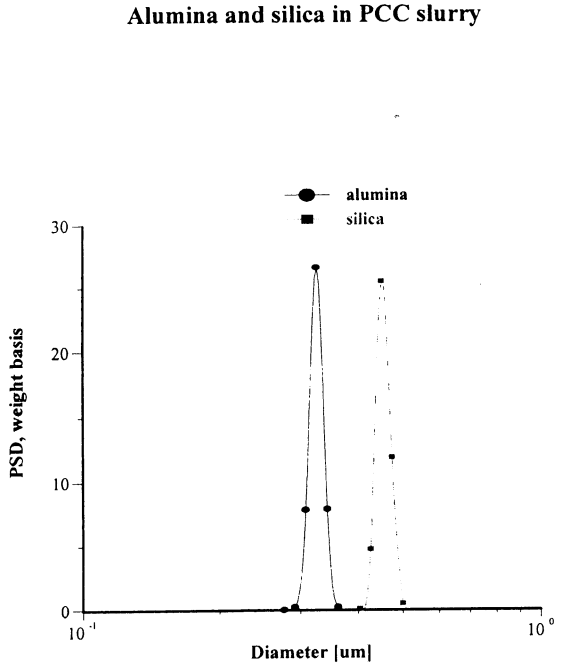

Fig. 20. Particle size distribution calculated using 'effective medium model'. The case of alumina AKP-30 and silica in the PCC dispersion as effective medium.

It is seen that in the case of the zirconia–alumina mixture a superposition PSD generates an attenuation spectrum that fits experimental spectra much better than the best 'multi-phase model' analysis PSD. The fitting error has improved from 5 to 2.3% and becomes comparable with the best fitting errors of the 'effective medium' model. This correlation between Prediction and Experiment proves that our concern about using a common standard deviation for both modes was well founded. The Prediction program allows us to apply independent standard deviation for each mode of the PSD and as a result we achieve much better fitting than in the case of the Analysis 'multi-phase' model that uses the same standard deviation for both modes.

In addition we conclude that there is no aggregation between the alumina and zirconia particles in this mixed dispersion. Otherwise, the theoretical attenuation based on the superposition assumption would not fit experimental data.

The situation with the second mixture (PCC–silica) is very different. In this case the predicted attenuation provides a much worse fit than the best 'multi-phase' model analysis. The fitting error degrades from 8 to 17.2%. This means that superposition assumption is not valid. In this case there is apparently some aggregation between the PCC and silica particles.

11. Structured dispersions

In many real concentrated dispersions particles build a structural network. They are not independent in these systems and oscillation of this network causes the additional mechanism of the sound attenuation: 'structural losses'. This complicates characterization of the particle size distribution. Fortunately, in many cases structural losses are negligible even at very high volume fractions. For instance, experimental dilution test with concentrated rutile and silica [13] dispersions yields correct particle size taking into account only viscous losses.

However, there are some instances when theory of viscous losses only fails to fit the experimental data. One such examples is given in the paper of

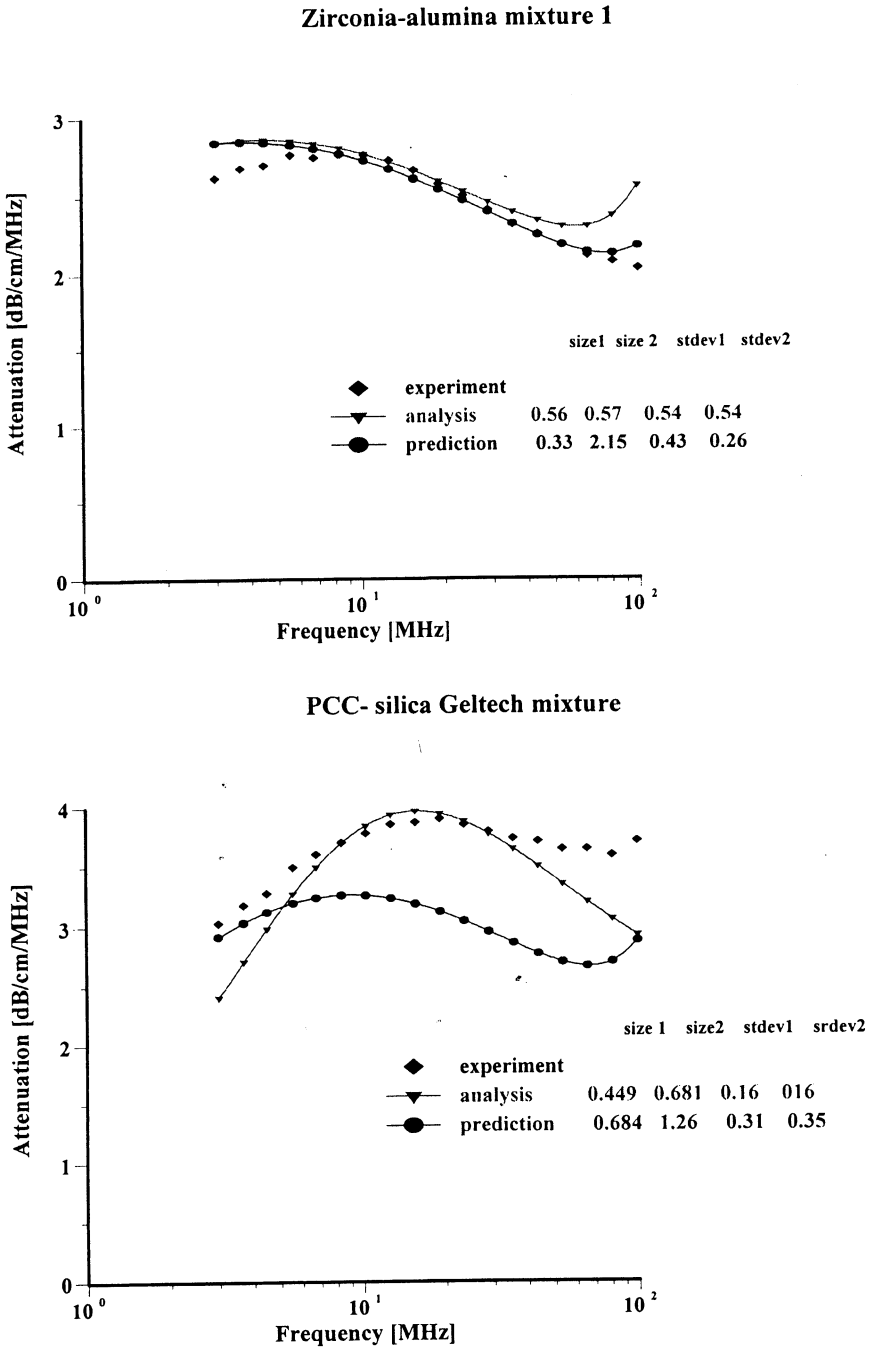

Fig. 21. Experimental and theoretical attenuation for zirconia–alumina mixture 1 and PCC–silica mixture. Theoretical attenuations are calculated for the best Analysis result and for combined PSD build from the individual distributions assuming no particle aggregation.

Table 6
Particle size of the two alumina samples

	Median particle size [micron]	
	ALM-41-01	AL-160SG-4
Size, horiba	1.47	0.56
Size, sympatec	1.98	0.71
Size, penkem, vfr < 20%	1.79	0.52
Size, acoustics, vfr = 40% with structural losses	1.63 (fit error 6.1%)	0.77 (fit error 2.3%)
Size, acoustics, vfr = 40% no structural losses	1.07 (fit error 19.2%)	0.8 (fit error 18.4%)

several Japanese scientists [65] from the National Institute for Resources and Environment, Tsukuba, Japan. We have used this paper in order to show that the additional mechanism of structural losses provides required theoretical framework for characterizing particle size distribution in the highly concentrated (up to 40 vol.%) and not completely stable dispersions.

The two alumina powders were used: Showa Denko AL-160SG-4 and Sumitomo Chemical Industry ALM-41-01. The median size of the each powder was measured by laser diffraction using a Sympatec Helos and by photo-centrifugation using a Horiba CAPA-700. This data is summarized in Table 6.

Both samples were stabilized with sodium polycalboxyl acid as a surfactant and ball milled for 3 days. The volume fractions of the slurries varied from 1 to 40%.

They used PenKem Acoustophor 8000 for measuring the acoustic attenuation spectra of these slurries. The particle size calculated from these attenuation spectra agreed with independent measurements at volume fractions below 20%. This size data is summarized in Table 6.

The attenuation at the highest volume fraction is shown on Fig. 22. We have reproduced these curves from the published graphs because the numerical data was not available in their paper. As a result, one may assume some small deviations from the original data.

We use attenuation spectra at the highest volume fraction in the further analysis.

Fig. 23 shows the experimental and theoretical attenuation spectra at the highest volume fractions, about 40 vol.% for both alumina samples. It is seen that the theory does not fit the experimental data very well since the experimental attenuation exceeds the theory by a substantial degree. Based on this excess, the authors concluded that there is an unknown factor which becomes significant at high volume fraction.

We suggest 'structural losses' as this hypothetical factor. We used Eq. (11) for calculating the theoretical attenuation spectra. We assumed that the first virial coefficient β is zero. The second virial coefficient is then used as an adjustable parameter in addition to median size and standard deviation of the lognormal particle size distribution. This searching routine looks for the particle size distribution which generates a theoretical attenuation spectra which fits the experimental spectra with the least error.

The addition of this new adjustable parameter, δ, allowed us to achieve much better theoretical fit as illustrated in Fig. 24. Table 6 gives the results of the calculated particle sizes and fitting errors. It

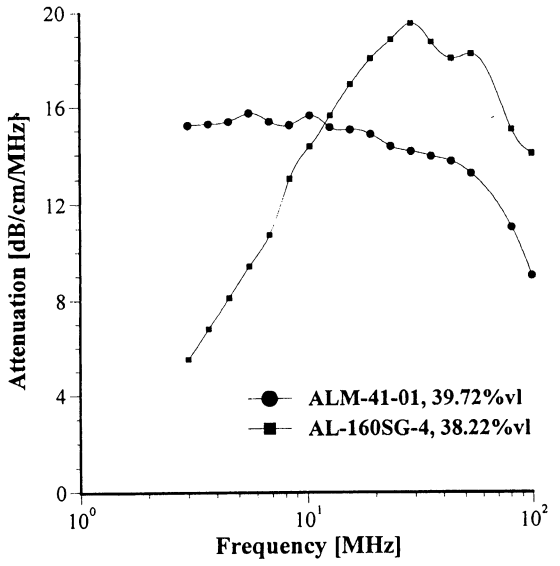

Fig. 22. Experimental attenuation spectra of the two alumina slurries characterized in the paper [65].

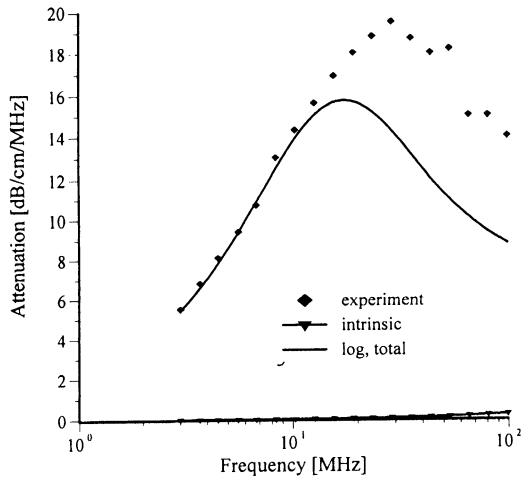

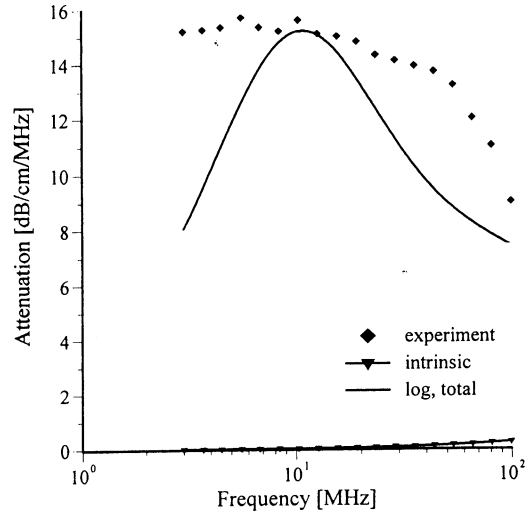

Fig. 23. Theoretical fit to the experimental data presented in the paper [65] assuming no structural losses.

is seen that the addition of these structural losses leads to dramatic improvements in the fitting error, which strongly suggests that this mechanism can indeed explain the observed excess attenuation.

The particle size data (Fig. 25) confirms this conclusion as well. It is seen that particle size calculated including these structural losses are much closer to independent measurement per-

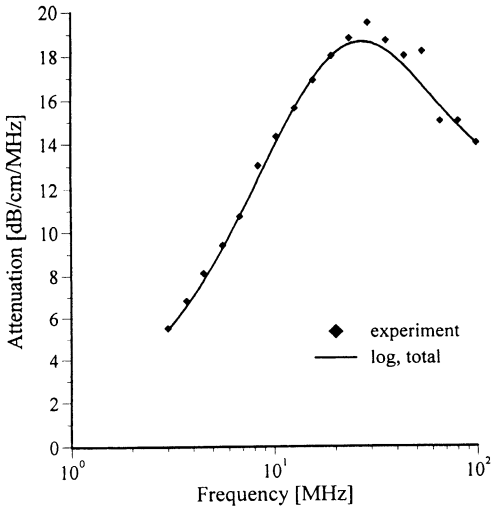

Fig. 24. Theoretical fit to the experimental data presented in the paper [65] with structural losses.

formed with diluted system using light based instruments.

It is interesting that the value of the second virial coefficient turns out to be the same for both samples, 0.8. It is independent on the particle size, as it is supposed to be. This parameter characterizes flexibility of reology of the polymer chains linking particles together into the structure at high volume fractions.

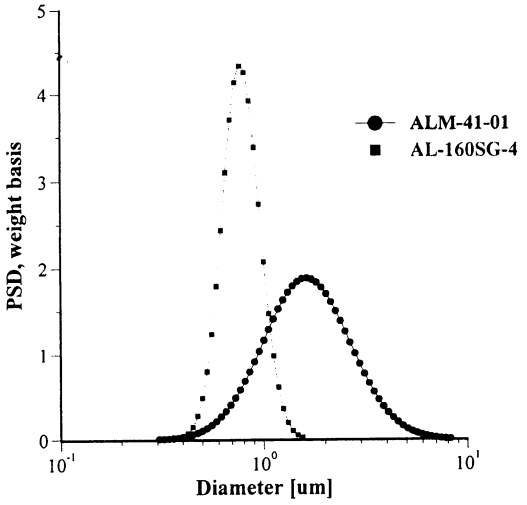

Fig. 25. Particle size distribution calculated for the two alumina samples described in the paper [65].

We would like to finish with warning, that addition of the structural losses is justified only when traditional theory fails and experiment shows an excess attenuation. This excess attenuation is a source of experimental information for calculating microreolgical properties.

12. Conclusions

In the last few years, the fields of acoustics and electroacoustics have made significant advancements in theoretical modeling, instrumentation, and experimental applications. The measurement of particle size by acoustic attenuation has been improved by new theoretical models that account for specific particle–particle interactions in concentrated structured systems and mixed dispersions. Refinements in the analysis of the different acoustic loss mechanisms have been presented in detail.

The combination of acoustic and electroacoustic spectroscopy provides more reliable and complete characterization of the disperse system than either one of those spectroscopes separately. Electroacoustic phenomena is more complicated when compared to acoustics because an additional electric field is involved. This problem becomes even more pronounced for concentrated systems and the best approach is to use acoustic attenuation to determine particle size, and electroacoustics separately to measure electric surface properties. The combined measurement of particle size and surface charge by the ESA technique requires a higher degree of theoretical complexity and can be less reliable.

New applications of the acoustic attenuation method and the colloid vibration current include ceramics, bimodal systems, chemical polishing materials, emulsions, microemulsions, latex, structured dispersions, mixed dispersions, clays, minerals, paints, inks, etc. Further applications of these techniques are underway especially in the field of non-aqueous systems that cannot be easily studied by other methods. While theoretical models have made great advancements, more work is needed to extend electroacoustic theory to non-aqueous systems and for explaining the role of the thermal effects in the electroacoustics.

List of abbreviations

a	particle radius
b	cell radius
C_p	heat capacity at constant pressure
c	sound speed
Du	Dukhin number
d	particle diameter
E	external electric field
$\langle E \rangle$	macroscopic electric field strength
F_f	hydrodynamic friction force
K	conductivity attributed with index
I_r	local current in the cell
$\langle I \rangle$	macroscopic current
I	intensity of the sound
j	complex unit
h	special function (Appendix A)
H	special function (Appendix A)
l	complex wave number
l_i	cell layer thickness
L	gap in the electroacoustic chamber
M^*	stress modulus
N	number of the volume fractions
P	pressure
r	spherical radial coordinate
t	time
S_{exp}	measured electroacoustic signal
u	speed of the motion attributed according to the index
Z	acoustic impedance
α	attenuation specified with index
β	thermal expansion attributed with index
δ_v	viscous depth
δ_t	thermal depth
ε	dielectric permettivity of the media
ε_0	dielectric permittivity of the vacuum
ϕ	electric potential
γ	hydrodynamic friction coefficient
η	dynamic viscosity
φ	volume fraction
κ	reciprocal Debye length
κ^σ	surface conductivity
λ	wave length
μ_d	dynamic electrophoretic mobility
ν	kinematic viscosity
θ	spherical angular coordinate

ρ	density attributed according to the index
τ	heat conductance attributed according to the index
ω	frequency
ζ	electrokinetic potential
Ω	drag coefficient

Indexes

i	index of the particle fraction
p	particles
m	medium
s	dispersion
r	radial component
θ	tangential component
vis	viscous
th	thermal
sc	scattering
int	intrinsic
in	acoustic input
out	acoustic output
rod	delay rod properties

Appendix A. Special functions

There are several special functions used in the above mentioned theory. They are specified below.

$$H(\alpha)=\frac{ih(\alpha)}{2\alpha}-\frac{i\mathrm{d}h(x)}{2\mathrm{d}x}_{x=\alpha}$$

$$h(x)=h_1(x)\,h_2(\beta)-h_1(\beta)\,h_2(x)$$

$$I=I(\beta)-I(\alpha)$$

$$I(x)=-h_1(\beta)\mathrm{e}^{x(1+j)}\left[\frac{3(1-x)}{2\beta^3}+j\left(\frac{x^2}{\beta^3}-\frac{3x}{2\beta^3}-\frac{1}{x}\right)\right]+h_2(\beta)\mathrm{e}^{-x(1+j)}\left[\frac{3(1+x)}{2\beta^3}+j\left(\frac{x^2}{\beta^2}+\frac{3x}{2\beta^3}-\frac{1}{x}\right)\right]$$

$$I_1=-j\frac{\mathrm{e}^{-x(1+j)}}{x}{}_{x=a}^{x=b}$$

$$I_2=-j\frac{\mathrm{e}^{x(1+j)}}{x}{}_{x=a}^{x=b}$$

$$I_{13}=-\frac{\mathrm{e}^{-x(1+j)}}{b^3}[1.5(x+1)+j(x^2+1.5x)]_{x=a}^{x=b}$$

$$I_{23}=\frac{e^{x(1+j)}}{b^3}[1.5(x-1)+j(-x^2+1.5x)]_{x=a}^{x=b}$$

$$h_1(x)=\frac{\exp(-x)}{x}\left[\frac{x+1}{x}\sin x-\cos x+j\left(\frac{x+1}{x}\cos x+\sin x\right)\right]$$

$$h_2(x)=\frac{\exp(x)}{x}\left[\frac{x-1}{x}\sin x+\cos x+j\left(\frac{1-x}{x}\cos x+\sin x\right)\right]$$

References

[1] J.R. Pellam, J.K. Galt, Ultrasonic propagation in liquids: application of pulse technique to velocity and absorption measurement at 15 magacycles, J. Chem. Phy. 14 (10) (1946) 608–613.

[2] C.T.J. Sewell, The extinction of sound in a viscous atmosphere by small obstacles of cylindrical and spherical form, Phil. Trans. Roy. Soc., London 210 (1910) 239–270.

[3] P.S. Epstein, R.R. Carhart, The absorption of sound in suspensions and emulsions, J. Acoust. Soc. Am. 25 (3) (1953) 553–565.

[4] D.J. McClements, Ultrasonic characterization of emulsions and suspensions, Adv. Colloid Interface Sci. 37 (1991) 33–72.

[5] Ultrasonic and Dielectric characterization techniques for suspended particultes, in: V.A. Hackley, J. Texter (Eds.), The American Chemical Society, Ohio, 1998.

[6] J. Lyklema, Fundamentals of Interface and Colloid Science, vol. 1, Academic Press, 1993.

[7] R.J. Hunter, Foundations of Collid Science, Oxford University Press, Oxford, 1989.

[8] H. Dhadwal, R. Ansari, W. Mayer, Rev. Sci. Instrum. 62 (12) (1991) 2963.

[9] A.S. Dukhin, P.J. Goetz, Acoustic spectroscopy for concentrated polydisperse colloids with high density contrast, Langmuir 12 (21) (1996) 4987–4997.

[10] A.S. Dukhin, P.J. Goetz, Characterization of aggregation phenomena by means of acoustic and electroacoustic spectroscopy, Colloids and Surfaces 144 (1998) 49–58.

[11] P. Debye, J. Chem. Phys. 1 (1933) 13.

[12] R.J. Hunter, Review. Recent developments in the electroacoustic characterization of colloidal suspensions and emulsions, Colloids and Surfaces 141 (1998) 37–65.

[13] A.S. Dukhin, V.N. Shilov, H. Ohshima, P.J. Goetz, Electroacoustics phenomena in concentrated dispersions. New theory and CVI experiment, Langmuir 15 (20) (1999) 6692–6706.
[14] A.S. Dukhin, P.J. Goetz, Acoustic and electroacoustic spectroscopy, Langmuir 12 (19) (1996) 4336–4344.
[15] T.A. Strout, Attenuation of sound in high-concentration suspensions: development and application of an oscillatory cell model, A Thesis, The University of Maine, 1991.
[16] U. Riebel, et al., The fundamentals of particle size analysis by means of ultrasonic spectrometry, Part. Part. Syst. Charact. 6 (1989) 135–143.
[17] A.H. Harker, J.A.G. Temple, Velocity and attenuation of ultrasound in suspensions of particles in fluids, J. Phys. D.: Appl. Phys. 21 (1988) 1576–1588.
[18] R.L. Gibson, M.N. Toksoz, Viscous attenuation of acoustic waves in suspensions, J. Acoust. Soc. Am. 85 (1989) 1925–1934.
[19] J. Happel, H. Brenner, Low Reynolds Number Hydrodynamics, Martinus Nijhoff Publishers, Dordrecht, The Netherlands, 1973.
[20] A.S. Dukhin, V.N. Shilov, Yu. Borkovskaya, Dynamic electrophoretic mobility in concentrated dispersed systems. Cell model, Langmuir 15 (10) (1999) 3452–3457.
[21] H.P. Pendse, T.C. Bliss, Wei Han, Particle shape effects and active ultrasound spectroscopy, in: V.A. Hackley, J. Texter (Eds.), Ultrasonic and Dielectric Characterization Techniques for Suspended Particulates, American Ceramic Society, Westerville, OH, 1998.
[22] Dispersion Technology Web Site www.dispersion.com
[23] J. Happel, Viscous flow in multiparticle systems:Slow motion of fluids relative to beds of spherical particles, AICHE J. 4 (1958) 197–201.
[24] S. Kuwabara, The forces experienced by randomly distributed parallel circular cylinders or spheres in a viscous flow at small reynolds numbers, J. Phys. Soc. Japan 14 (1959) 527–532.
[25] V.N. Shilov, N.I. Zharkih, Yu.B. Borkovskaya, Theory of nonequilibrium electrosurface phenomena in concentrated disperse system.1. Application of nonequilibrium thermodynamics to cell model, Colloid J. 43 (3) (1981) 434–438.
[26] M.W. Kozak, J.E. Davis, Electrokinetic phenomena in fibrous porous media, JCIS 112 (2) (1986) 403–411.
[27] S. Levine, G.H. Neale, The prediction of electrokinetic phenomena within multiparticle systems.1. Electrophoresis and electroosmosis, J. Colloid Interface Sci. 47 (1974) 520–532.
[28] J.R. Allegra, S.A. Hawley, Attenuation of sound in suspensions and emulsions:theory and experiments, J. Acoust. Soc. Am. 51 (1972) 1545–1564.
[29] J.D. McClements, Ultrasonic determination of depletion flocculation in oil-in-water emulsions containing a nonionic surfactant, Colloids and Surfaces 90 (1994) 25–35.
[30] D.J. McClements, Comparison of multiple scattering theories with experimental measurements in emulsions, J. Acoust. Soc. Am 91 (2) (1992) 849–854 February.
[31] A.K. Holmes, R.E. Challis, D.J. Wedlock, A wide-bandwidth study of ultrasound velocity and attenuation in suspensions: comparison of theory with experimental measurements, J. Colloid Interface Sci. 156 (1993) 261–269.
[32] A.K. Holmes, R.E. Challis, D.J. Wedlock, A wide-bandwidth ultrasonic study of suspensions: The variation of velocity and attenuation with particle size, J. Colloid Interface Sci. 168 (1994) 339–348.
[33] A.S. Dukhin, P.J. Goetz, C.W. Hamlet, Acoustic spectroscopy for concentrated polydisperse colloids with low density contrast, Langmuir 12 (21) (1996) 4998–5004.
[34] A.S. Dukhin, J.P. Goetz, T.H. Wines, P. Somasundaran, Acoustic and electroacoustic Spectroscopy, Colloids and Surfaces, A, 2000.
[35] L.W. Anson, R.C. Chivers, Thermal effects in the attenuation of ultrasound in dilute suspensions for low values of acoustic radius, Ultrasonic 28 (1990) 16–25.
[36] M.A.Zh. Isakovich, Exp. Theor. Phys. 18 (1948) 907.
[37] P.S. Waterman, R. Truell, J. Math. Phys. 2 (1961) 512.
[38] R. Chanamai, J.N. Coupland, D.J. McClements, Effect of temperature on the ultrasonic properties of oil-in-water emulsions, Colloids and Surfaces 139 (1998) 241–250.
[39] S. Temkin, Sound speed in suspensions in thermodynamic equilibrium, Phys. Fluids 4 (11) (1992) 2399–2409 November.
[40] S. Temkin, Sound propagation in dilute suspensions of rigid particles, J. Acoust. Soc. Am. 103 (2) (1998) 838–849 February.
[41] F. Booth, J. Enderby, On electrical effects due to sound waves in colloidal suspensions, Proc. Am. Phys. Soc. 208A (1952) 32.
[42] J.A. Enderby, On electrical effects due to sound waves in colloidal suspensions, Proc. Roy. Soc., London A207 (1951) 329–342.
[43] B.J. Marlow, D. Fairhurst, H.P. Pendse, Colloid vibration potential and the electrokinetic characterization of concentrated colloids, Langmuir 4 (1983) 611–626.
[44] S.S. Dukhin, B.V. Derjaguin, Electrokinetic phenomena, in: E. Matijevic (Ed.), Surface and Colloid Science, John Wiley & Sons, NY, 1974, p. 7.
[45] R.W. O'Brien, Electro-acoustic effects in a dilute suspension of spherical particles, J. Fluid Mech. 190 (1988) 71–86.
[46] R.W. O'Brien, Determination of particle size and electric charge, US Patent 5,059,909, Oct. 22, 1991.
[47] H. Ohshima, Dynamic electrophoretic mobility of spherical colloidal particles in concentrated suspensions, J. Colloid Interface Sci. 195 (1997) 137–148.
[48] A.S. Dukhin, H. Ohshima, V.N. Shilov, P.J. Goetz, Electroacoustics for concentrated dispersions, Langmuir 15 (10) (1999) 3445–3451.
[49] H. Ohshima, A.S. Dukhin, Colloid vibration potential in a concentrated suspension of spherical colloidal particles, J. Colloid Interface Sci. 212 (1999) 449–452.
[50] A.S. Dukhin, V.N. Shilov, H. Ohshima, P.J. Goetz, Electroacoustics Phenomena in Concentrated Dispersions, Effect of the Surface Conductivity, Langmuir, submitted.

[51] S.S. Dukhin, V.N. Shilov, Dielectric Phenomena and the Double Layer in Disperse Systems and Polyelectrolytes, John Wiley & Sons, NY, 1974.
[52] A.S. Dukhin, P.J. Goetz, Particle size distribution in structured concentrated slurries, Langmuir, submitted.
[53] A.S. Dukhin, P.J. Goetz, Method and device for characterizing particle size distribution and zeta potential in concentrated system by means of Acoustic and Electroacoustic Spectroscopy, patent USA, pending.
[54] A.S. Dukhin, P.J. Goetz, Method and device for determining particle size distribution and zeta potential in concentrated dispersions, patent USA, pending.
[55] A.S. Dukhin, P.J. Goetz, Acoustic and Electroacoustic Spectroscopy for Characterizing Concentrated Dispersions and Emulsions, Adv. Colloid and Interface Sci., 2000.
[56] A.S. Dukhin, P.J. Goetz, S.Truesdail, Titration of concentrated dispersions using electroacoustic ζ-potential probe, Langmuir, submitted.
[57] A.S. Dukhin, P.J. Goetz, Characterization of concentrated dispersions with several dispersed phases by means of acoustic spectroscopy, Langmuir, submitted.
[58] A.J. Babchin, R.S. Chow, R.P. Sawatzky, Electrokinetic measurements by electroacoustic methods, Adv. Colloid Interface Sci. 30 (1989) 111.
[59] R.P. Sawatzky, A.J. Babchin, Hydrodynamics of electrophoretic motion in an alternating electric field, J. Fluid. Mech. 246 (1993) 321–334.
[60] Shin-ichi Takeda, P.J. Goetz, Dispersion/flocculated size characterization of alumina particles in highly concentrated slurries by ultrasound attenuation spectroscopy, Colloids and Surfaces 143 (1998) 35–39.
[61] Takeda, Shin-ichi, T. Chen, P. Somasundaran, Evaluation of particle size distribution for nanosized particles in highly concentrated suspensions by ultrasound attenuation spectroscopy, Colloids and Surfaces, 1999.
[62] Takeda, Shin-ichi, Characterization of ceramic slurries by ultrasonic attenuation spectroscopy, in: V.A. Hackley, J. Texter (eds.), Ultrasonic and Dielectric Characterization Techniques for Suspended Particulates, American Ceramic Society, Westerville, OH, 1998.
[63] A.S. Dukhin, P.J. Goetz, Characterization of chemical polishing materials (monomodal and bimodal) by means of acoustic spectroscopy, Colloids and Surfaces, accepted.
[64] T.H. Wines, A.S. Dukhin, P. Somasundaran, Acoustic spectroscopy for characterizing heptane/water/AOT reverse microemulsion, JCIS 216 (1999) 303–308.
[65] T. Hayashi, H. Ohya, S. Suzuki, S. Endoh, Errors in size distribution measurement of concentrated alumina slurry by ultrasonic attenuation spectroscopy, J. Soc. Powder Techn., Japan, 498–504 (2000).